

# The anatomy of the NGC 5044 group – I. Group membership and dynamics

J. Trevor Mendel<sup>\*</sup>, Robert N. Proctor, Duncan A. Forbes, Sarah Brough

*Centre for Astrophysics & Supercomputing, Mail H39, Swinburne University, Hawthorn, VIC 3122, Australia*

29 October 2018

## ABSTRACT

We use a combination of new AAOmega multi-object wide-field spectroscopic observations and literature data to define 111 spectroscopically confirmed members of the massive NGC 5044 group with  $M_B \leq -13.5$  mag, providing a three-fold increase in group members over previous analyses of this group. We find the group to have a dynamical mass of  $9.2 \times 10^{14} M_\odot$ , placing it on the border between rich groups and poor clusters. However, comparison to the  $L_X$ - $\sigma_v$  and  $L_X$ -Mass relations shows it more closely follows cluster scaling relations. Using a combination of crossing time, X-ray contours and line-of-sight velocity profile we are able to preclude growth of the NGC 5044 group via major sub-group mergers within the last  $\sim 1$  Gyr. While the majority of dynamical indicators for the group suggest it is virialized, we find evidence for a small, dynamically distinct sub-group at 1.4 Mpc from the group centre, suggesting that the NGC 5044 group is the dominant structure in its local environment, and is currently accreting smaller groups.

**Key words:** galaxies: clusters: NGC 5044 group - galaxies: distances and redshift - galaxies: fundamental parameters - galaxies: formation - galaxies: evolution

## 1 INTRODUCTION

It is well known that our own Galaxy is not isolated, residing with M31 and a host of smaller galaxies in the Local Group. Large area surveys have confirmed that the Local Group is not exceptional, but rather representative of an extremely common environment (e.g. Geller & Huchra 1983; Eke *et al.* 2004; Weinmann *et al.* 2006). However, despite the apparent commonality of the group environment, the astrophysical processes acting within groups and their effects on observed galaxy populations are relatively poorly understood. This is due to both the low galaxy numbers and galaxy surface densities typically associated with groups that make them observationally expensive.

Consequently, it is observations of galaxy clusters that have largely driven our current understanding of environmental effects on galaxy populations, namely that galaxies in clusters are redder (e.g. Butcher & Oemler 1984) and morphologically earlier types (e.g. Dressler 1980) relative to galaxies in the field. The expected correlation of star formation rate with density, based on the morphology-density and morphology-radius relations, has led observers to measure star formation rates as a function of environment in large samples such as the 2dFGRS (e.g. Lewis *et al.* 2002)

and SDSS (e.g. Gómez *et al.* 2003). These authors have found that star formation rates decrease as one moves from the field to cluster environment. Perhaps more interestingly, however, is that the observed star formation truncation is associated with local density rather than physical proximity to a cluster, and therefore the physical mechanisms responsible are acting primarily in lower density, group-like environments. This has been confirmed by studies attempting to link field and cluster galaxies, which find observed cluster populations cannot be generated directly from the accretion of field galaxies. Galaxy groups, therefore, *must* be playing a significant role as an intermediary stage in galaxy evolution (e.g. Kodama & Smail 2001; Fujita 2003).

After initial violent relaxation where galaxies are dominated by a collective potential (Lynden-Bell 1967), the dynamics of group and cluster galaxies are predominantly affected on more local scales. Of the several possible mechanisms driving galaxy evolution, those dependent on the size of the potential well (e.g. harassment; Moore 1996) or density of the intra-cluster medium (e.g. ram-pressure stripping; Gunn & Gott 1972) will be most effective in clusters. Conversely, the low-velocity group environment favours mergers as the preferred method of relaxation due to the growing efficiency of dynamical friction at low relative velocities.

It has been shown that mergers can lead to both morphology and luminosity segregation (Fusco-Femiano &

<sup>\*</sup> tmendel@astro.swin.edu.au

Menci 1998; Yepes, Domínguez-Tenreiro & Del Pozo-Sanz 1991), and observations suggest that galaxies are segregated in both groups (Mahdavi *et al.* 1999; Girardi *et al.* 2003) and clusters (Adami, Biviano & Mazure 1998; Biviano *et al.* 2002; Lares, Lambas & Sánchez 2004). Since mergers will also affect the relative number of galaxies at a given luminosity, one might expect the prevalence of mergers in groups to influence the shape of the group luminosity function. This is, in fact, a possible explanation of the commonly observed “dip”, indicative of intermediate mass galaxies merging to form more luminous ones (e.g. Trentham & Tully 2002; Miles *et al.* 2004). It is also worth noting that recent observations of ram-pressure stripping in groups (e.g. Bureau & Carignan 2002; Kantharia *et al.* 2005; Rasmussen, Ponman & Mulchaey 2006) support the results of numerical simulations which suggest that group-level ram-pressure stripping could also play some role in group galaxy evolution (Hester 2006).

Typical studies of poor groups may classify 10-20 galaxies as group members, the majority of which have had their membership assigned using photometric or morphological criteria. More robust studies have included only galaxies for which recession velocity measurements are available (e.g. Zabludoff & Mulchaey 1998; Carlberg *et al.* 2001; Brough *et al.* 2006a), however this often leads to the need to stack groups in order to measure their properties due to the low numbers of redshifts typically available. The problem with stacking groups, however, is that while it is then possible to constrain the generalised global properties of groups (e.g. mass distribution, velocity dispersion profile etc.) the individual properties of any single group are washed out.

Here we aim to address this issue by establishing the properties of the NGC 5044 group and its galaxies independently. By studying a single rich group we are able to examine evidence for dynamical segregation, substructure and peculiarities in its dynamical properties that are washed out when stacking multiple groups. In this paper, we present new deep spectroscopic data that allow us to spectroscopically confirm  $\sim 40$  new group members. With the addition of these velocities, we create a new list of 111 confirmed group members that then allows a comprehensive analysis of the dynamical attributes of the NGC 5044 group and its constituent galaxies out to nearly two virial radii. In future work we will use these data to examine the stellar populations of the group galaxies in relation to their position in the group, HI gas properties, star formation rates and dynamical properties.

This paper is organised as follows: in §2 and §3 we describe some general properties of the NGC 5044 group and the data set we have assembled. §4 describes the method we have used to select group members from our list of potential candidates. The global group properties are addressed in §5, and the properties related to individual galaxies are summarised in §6.

Throughout this paper we assume  $H_0 = 70 \text{ km s}^{-1} \text{ Mpc}^{-1}$  where applicable and recession velocities are quoted in terms of  $cz$ . We adopt the distance modulus of Tonry *et al.* (2001),  $(m - M)_0 = 32.31$  (28.99 Mpc), measured using surface brightness fluctuations with corrections applied to adjust for the improved Cepheid distance measurements of Jensen *et al.* (2003). Magnitudes have been corrected for galactic extinction using the dust

maps of Schlegel, Finkbeiner & Davis (1998). Following convention we use  $R$  to denote 2D, projected radii and  $r$  to indicate 3D, deprojected radii.

## 2 THE NGC 5044 GROUP

We have selected the NGC 5044 group as the focus of this work as it is our goal to describe the properties of a *single* group, and its large galaxy population is sufficient to perform a statistical analysis.

Ferguson & Sandage (1990, hereafter FS90; 1991, hereafter FS91) photometrically studied 7 nearby groups and clusters, including NGC 5044, constructing group luminosity functions and examining the relative fractions of dwarf and giant galaxies. In their work, FS91 show that the early-type dwarf to giant ratio (EDGR) correlates nearly monotonically with richness. The intermediate richness of the NGC 5044 group, means that its EDGR occupies the transition between groups and clusters. They also found evidence for a steep faint-end luminosity function in the NGC 5044 group, however their photometric selection is likely to contain significant background contamination.

The NGC 5044 group has also been studied as part of the Group Evolution Multi-wavelength Survey (GEMS; Osmond & Ponman 2004; Forbes *et al.* 2006) and so has been observed at both X-ray and HI wavelengths (Osmond & Ponman 2004; McKay *et al.* 2004; Kilborn *et al.* in preparation, hereafter K08). The GEMS group sample was selected from the availability of ROSAT PSPC pointings. Further X-ray observations of the NGC 5044 group have been carried out using both Chandra and XMM-Newton (Buote *et al.* 2003; Tamura *et al.* 2003; Buote, Brighenti & Mathews 2004). These authors found the group to have a cool-core component of  $\sim 0.7 \text{ keV}$  within 10 kpc (consistent with the kinetic temperature of stars in NGC 5044 itself), and a warmer 1.4 keV outside of 40 kpc (characteristic of the group halo). The large radial extent of X-ray emission ( $r > 60 \text{ kpc}$ ) and high  $L_X/L_B$  ratio ( $\log_{10} L_X/L_B = 31.82 \pm 0.01 \text{ ergs s}^{-1} L_\odot^{-1}$ ; Osmond & Ponman 2004) are key indications that the hot gas is associated with a group sized potential rather than just NGC 5044 itself.

## 3 SAMPLE SELECTION AND DATA

### 3.1 AAOmega observations

We used the photometrically determined NGC 5044 group catalogue of FS90 as the target list for new spectral observations. The FS90 catalogue was constructed using photographic plates covering  $\sim 2.3 \text{ deg}^2$  taken at the 2.5m duPont Telescope at the Las Campanas Observatory. AAOmega’s  $3 \text{ deg}^2$  field-of-view allowed us to observe all 162 objects in the FS90 NGC 5044 group catalogue simultaneously.

FS90 used a B-band radial cut of  $16''$ , estimated to be  $27 \text{ mag arcsec}^{-2}$  at the distance of NGC 5044, to limit background contamination. Group membership was then defined using morphological criteria to differentiate between background galaxies and genuine group members. The FS90 sample for NGC 5044 is complete to  $B_T \sim 18$ , and complete at the 90% level to  $B_T \sim 19$ .

Our spectroscopic observations of the NGC 5044 group

were obtained in 2006 March on the 25–27<sup>th</sup> using the AAOmega multi-object spectrograph at the 3.9m *Anglo-Australian Telescope* (AAT). Spectra were taken using medium resolution 580V and 385R gratings, yielding dispersions of 3.5 Å and 5.3 Å FWHM respectively and spectral coverage from 3700–8800 Å.

Since the targets spanned a wide range in magnitude ( $-19.3 \leq M_B \leq -12.3$ ) observations were divided into two separate plate configurations to limit the effects of scattered light from the brightest sources. Plate configurations used a total of 197 fibres, 162 allocated to targets and 35 placed on blank sky regions. Bright (faint) target observations were carried out in a series of 20 (30) minute integrations, with a total of 3–4 such integrations per plate configuration, for a total of 4 (17) hours of observation across the 3 observing nights.

Data were reduced using the 2DFDR software supplied and maintained by the Anglo Australian Observatory. This software handles over-scan subtraction, identification of the fibre apertures, fibre flat-fielding and throughput calibration, wavelength calibration, median sky subtraction and co-addition of science frames. Due to known sensitivity issues in the blue arm of AAOmega at the time of observing ( $\sim 50\%$  decrease from expected), many of the faintest objects were lost in the co-addition process as the reduced throughput resulted in these fibres being read-noise dominated.

Recession velocities were measured using the Fourier cross-correlation routine, FXCOR, in IRAF. These recession velocity measurements were made for blue and red frames separately to verify the spectral wavelength solutions and recession velocity measurements. Cross-correlations were performed using both absorption (standard stars) and emission (rest frame emission galaxy) templates. We preferentially use absorption line templates for cross-correlation, however in cases where absorption lines provided a poor redshift solution, emission templates were used. In this way, redshifts were measured for 103 galaxies out of the total 162 galaxy sample of FS90.

Fig. 1 shows the relationship between newly measured redshifts and those available in the NASA/IPAC Extragalactic Database (NED), showing the velocity difference between the two plotted against our measured velocities. Velocities are shown only for those galaxies for which we find recession velocities  $\leq 4000 \text{ km s}^{-1}$  (the range of interest for possible NGC 5044 group members), however background objects with higher velocities show similar good agreement with the literature. We find no evidence for systematic variations with recession velocity out to a redshift of  $\sim 0.7$  (our highest redshift object), however based on the median absolute deviation between our velocity measurements and those in NED we adopt a systematic uncertainty of  $50.7 \text{ km s}^{-1}$ .

### 3.2 6dFGS data

In order to include the most complete NGC 5044 group member list available, we have used supplementary data from the second data release of the 6dF Galaxy Survey (6dFGS DR2; Jones *et al.* 2005) to expand our AAOmega sample. The 6dFGS is a large,  $17046 \text{ deg}^2$  survey of southern sky targets selected from the 2MASS Extended Source Catalogue (Jarrett *et al.* 2000) to include all galaxies brighter than  $K_{\text{tot}} = 12.75 \text{ mag}$ . To our list of possible group

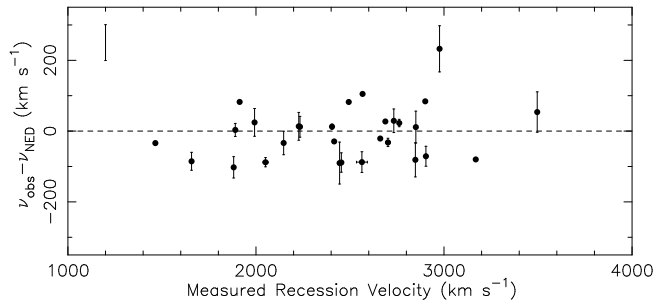


**Figure 1.** Comparison of recession velocities measured in this work with available data from NED. Only the 29 overlapping galaxies with measured recession velocities  $\leq 4000 \text{ km s}^{-1}$  are shown. The error bar in the upper left side of the figure represents our adopted systematic uncertainty of  $50.7 \text{ km s}^{-1}$ .

members we add all 6dFGS galaxies within 4 degrees of NGC 5044 ( $\sim 2 \text{ Mpc}$  in projected separation) and recession velocities between  $500$  and  $5000 \text{ km s}^{-1}$ , yielding 24 galaxies. As of 6dFGS DR2 the region surrounding NGC 5044 has not been surveyed completely, and so 6dFGS galaxies included here are not uniformly distributed. In particular, galaxies with declinations greater than  $\sim -15.25^\circ$  ( $\sim 0.65 \text{ Mpc}$  north of the group centre) are not present in the 6dFGS DR2 sample (see Fig. 5 for a more detailed footprint of 6dFGS coverage in this region).

### 3.3 GEMS HI data

The NGC 5044 group has been surveyed for neutral hydrogen as part of the GEMS project using the 20-cm multi-beam receiver on the Parkes radio telescope by K08 (see also McKay *et al.* 2004). They surveyed a  $5.5^\circ \times 5.5^\circ$  region centred roughly on NGC 5044 and identified 23 HI detections above a mass limit of  $1.8 \times 10^8 M_\odot$  (flux levels above  $18 \text{ mJy beam}^{-1}$ ). Of these, 5 represent new galaxy detections which have been confirmed using high resolution imaging from the Australian Telescope Compact Array (further details will be given in K08), and so these new galaxies are included in our velocity sample.

### 3.4 NED data

Given the incomplete spatial coverage available from the 6dFGS DR2 data we have supplemented these data using sources with known recession velocities from the NED in the same position and velocity range, providing 51 additional galaxies to our sample. The heterogeneous nature of the NED data means that an accurate estimate of incompleteness effects is difficult. However, Brough *et al.* (2006b) have shown NED to be complete in recession velocity and photometry to  $K < 11 \text{ mag}$ , with statistically similar results obtained when fainter magnitude objects are included.

In total, the combined AAOmega, 6dFGS, GEMS HI and NED data provide 152 galaxies with redshifts between  $500$  and  $5000 \text{ km s}^{-1}$  in the region of NGC 5044.

### 3.5 Photometric data

In order to supply a cross-reference for the B-band magnitudes of FS90, as well as supplementary B-band photometry

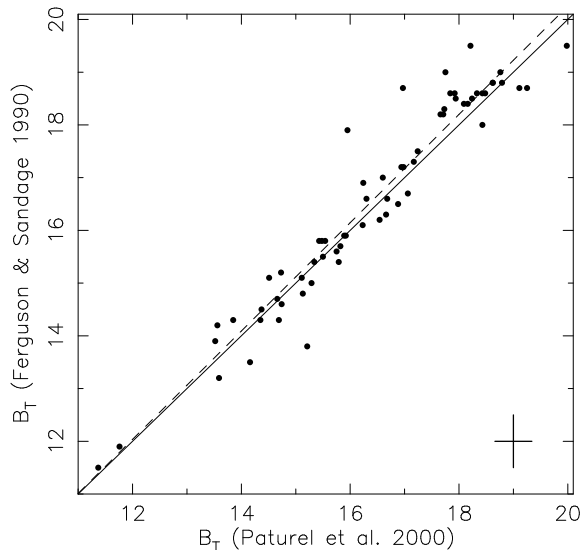


**Figure 2.** Photometric comparison between  $B_T$  as determined by FS90 and P00. Errors for each point are 0.5 and 0.34 mag as estimated by FS90 and P00 respectively, and are shown by the error bar in the lower right corner. The solid line represents the one-to-one line, while the dashed line represents a least squares fit to the data.

for galaxies not in the FS90 galaxy list (i.e. those selected from 6dFGS, K08 and NED) we have adopted additional B-band photometric data from Paturel *et al.* (2000; hereafter P00). They obtain  $B_T$  from Digitised Sky Survey (DSS) plates and provide total B-band magnitudes for 65 of the 162 galaxies in the FS90 NGC 5044 group sample, 21 out of 24 of our 6dFGS selected galaxies, 36 of the 51 NED galaxies, and 1 out of 5 from the K08 sample.

In Fig. 2 we show a comparison of FS90 and P00 total B-band magnitudes, showing the good agreement of the two  $B_T$  determinations. There is no evidence for any systematic offsets between the two samples. The r.m.s. scatters about the one-to-one and best fit lines are 0.38 and 0.37 mags respectively, and we therefore adopt the P00 magnitudes without additional correction when FS90 measurements are unavailable.

K-band magnitudes provide a reasonable proxy for stellar mass as they are relatively unaffected by dust extinction and young, hot stars. We have therefore compiled the available K-band photometry of our sample. The Two Micron All Sky Survey (2MASS, Skrutskie *et al.* 2006) has provided an excellent resource of K-band photometry for a large number of galaxies, and supplies total K-band magnitudes and isophotal radii ( $r_{K20}$ ) for 41 of the 162 galaxies in the FS90 target list and all 24 6dFGS selected galaxies.

To provide greater K-band coverage, we adopt additional magnitudes from the Deep Near Infrared Survey (DENIS; Paturel *et al.* 2005; hereafter P05). In Fig. 3 we show a comparison of 2MASS and P05 K-band magnitudes. The agreement between the two samples is good and there are no suggestions of systematic offsets. We preferentially use 2MASS K magnitudes, supplementing with P05 data where necessary.

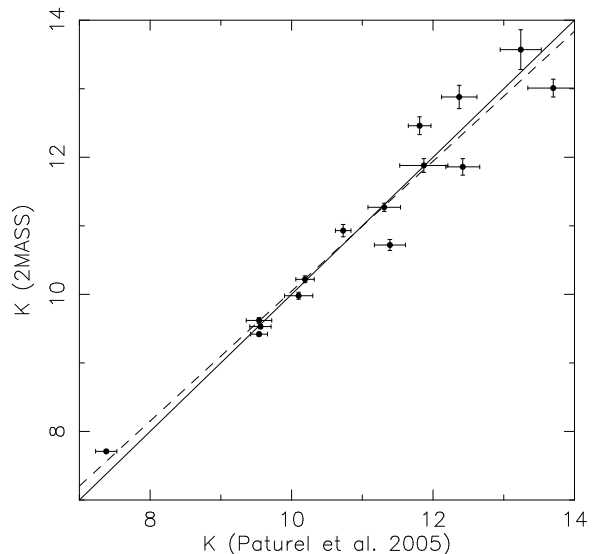


**Figure 3.** Photometric comparison between K-band magnitudes from 2MASS and DENIS (as measured by P05). Error bars represent 1- $\sigma$  deviations. The solid line represents the one-to-one line, while the dashed line represents a least squares fit to the data.

#### 4 GROUP MEMBERSHIP

Our AAOmega observations have allowed us to obtain new recession velocity measurements of a significant number of galaxies for which we need to assess group membership.

Brough *et al.* (2006a; hereafter B06) used data from NED and 6dFGS to define the NGC 5044 group using a friends-of-friends algorithm (FoF; Huchra & Geller 1982) which selects group members down to a specified galaxy density above the critical density (in their case,  $\delta=150\rho_0$ ). Groups derived using the FoF method are sensitive to the maximum allowed projected and velocity separation (i.e. the linking length and velocity), the sample luminosity function and the magnitude limit of the sample. The inhomogeneous nature of our combined sample means that no single luminosity function or magnitude limit will be adequate for selection of the group using an FoF algorithm, and we therefore adopt a clipping method as it requires no *a priori* assumptions regarding our data.

Membership of the NGC 5044 group is assigned using an iterated velocity dispersion clipping as follows. Galaxies are binned radially, using NGC 5044 as the centre, and a moving mean velocity and velocity dispersion,  $\sigma$ , are calculated. Galaxies with velocities greater than  $3\sigma$  from the moving mean are removed from the group member list and the process is repeated until no additional galaxies are removed.

Velocity clipping is particularly well suited to this sample as the NGC 5044 group is well separated in velocity space from background contamination, illustrated in Fig. 4. We have imposed a cut at 1.6 Mpc in projected radius, beyond which our moving velocity dispersion begins to rise due to increasing velocity outliers. It is likely that some of the galaxies beyond this cut are also group members, however we are unable to reliably separate genuine group members from contaminant galaxies, and so beyond this radius we no longer include galaxies as group members. We note that the inclusion or exclusion of galaxies in this region has a negli-

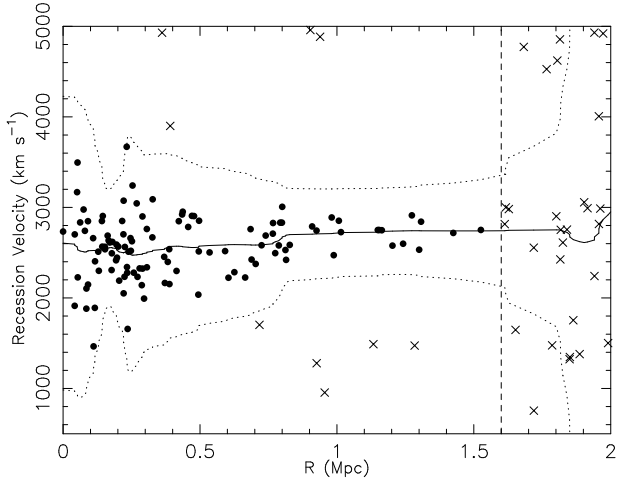


**Figure 4.** Galaxy recession velocities against their projected distance from NGC 5044. Circles and crosses represent galaxies included and excluded from the group respectively. The vertical dashed line shows a radial cut of 1.6 Mpc, beyond which galaxies are no longer considered as members. Dotted lines represent the  $3\sigma$  velocity limit of the data, with the solid line showing the moving mean velocity.

gible affect on the dynamical parameters we derive for the group (i.e. mass, crossing time etc.).

The member list for the NGC 5044 group is shown in Table 1 and includes 111 galaxies, including 71 from FS90, 16 from 6dFGS, 19 from NED and 5 from K08. In Fig. 5 we show the distribution of our confirmed group member galaxies on the sky, with symbols representing different morphological types.

The group properties we find using velocity clipping rather than FoF are consistent within uncertainties with those from B06.

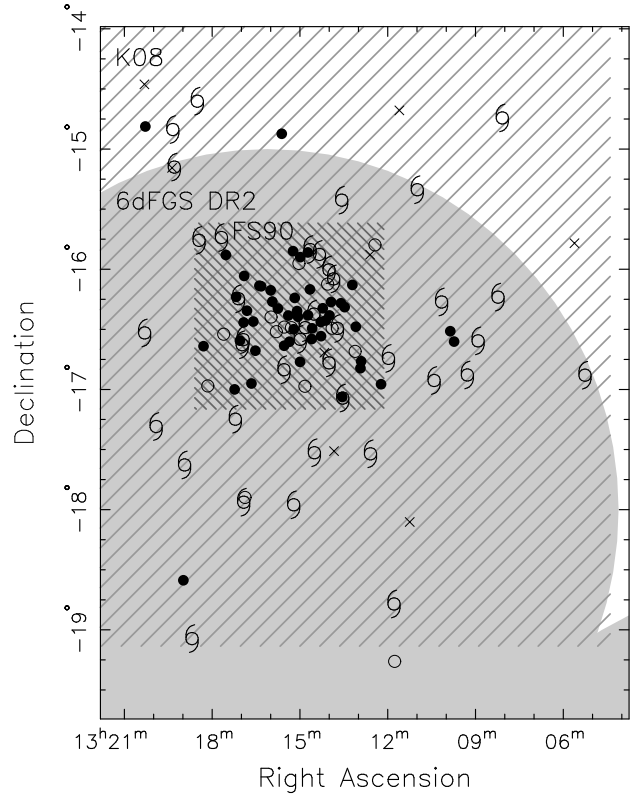


**Figure 5.** Distribution of confirmed group members on the sky. Filled circles, open circles and spirals represent elliptical, S0 and late type galaxies respectively. Crosses mark group members with unknown morphological types. The shaded and hashed regions indicate the areas covered by the K08, FS90 and 6dFGS data.

Table 1. Confirmed NGC 5044 Group Galaxies

| Galaxy Identifier | RA<br>(J2000) | DEC<br>(J2000) | $cz$<br>( $\text{km s}^{-1}$ ) | FS90<br>Memb. | $B_T$<br>(mag) | $K_T$<br>(mag) | Morphology          |
|-------------------|---------------|----------------|--------------------------------|---------------|----------------|----------------|---------------------|
| (1)               | (2)           | (3)            | (4)                            | (5)           | (6)            | (7)            | (8)                 |
| FS90 001          | 13 12 13.80   | -16 57 22.0    | 2036.4                         | 1             | 18.4           | ...            | dE,N?               |
| FS90 003          | 13 12 26.35   | -15 47 52.3    | 2904.0                         | 3             | 14.3           | 9.34±0.03      | Sb?                 |
| FS90 005          | 13 12 54.50   | -16 45 57.0    | 2454.2                         | 1             | 13.2           | 9.27±0.03      | E                   |
| FS90 007          | 13 12 56.10   | -16 49 22.0    | 2398.3                         | 1             | 19.2           | ...            | dE                  |
| FS90 009          | 13 13 05.49   | -16 28 41.7    | 1992.6                         | 1             | 14.5           | 10.58±0.06     | S0                  |
| FS90 011          | 13 13 06.80   | -16 41 00.0    | 2669.1                         | 1             | 18.9           | 14.30±0.46     | dSd(on edge)        |
| FS90 015          | 13 13 12.48   | -16 07 50.2    | 2761.8                         | 1             | 14.6           | 10.72±0.08     | E                   |
| FS90 017          | 13 13 28.42   | -16 18 52.9    | 2661.0                         | 2             | 15.6           | ...            | S0pec <sup>a</sup>  |
| FS90 018          | 13 13 32.24   | -17 04 43.4    | 2847.8                         | 1             | 14.3           | 9.98±0.05      | Sab                 |
| FS90 019          | 13 13 33.40   | -17 03 46.0    | 2298.2                         | 1             | 17.7           | 12.74±0.62     | dE                  |
| FS90 020          | 13 13 36.00   | -16 16 58.0    | 2341.1                         | 1             | 18.9           | ...            | dE,N                |
| FS90 022          | 13 13 43.10   | -16 29 58.0    | 2703.0                         | 1             | 18.9           | ...            | dE/ImV              |
| FS90 024          | 13 13 50.96   | -16 05 13.7    | 2521.0                         | 3             | 17.2           | ...            | Sm <sup>a</sup>     |
| FS90 027          | 13 13 54.15   | -16 29 27.4    | 2444.7                         | 1             | 14.2           | 9.81±0.05      | SB0 <sub>3</sub>    |
| FS90 029          | 13 13 56.21   | -16 16 24.3    | 2415.9                         | 1             | 15.5           | 11.78±0.13     | d:E                 |
| FS90 030          | 13 13 59.52   | -16 23 03.8    | 2493.3                         | 1             | 15.7           | ...            | dE <sup>a</sup>     |
| FS90 031          | 13 14 00.47   | -16 00 44.2    | 2278.7                         | 3             | 17.0           | ...            | Im <sup>a</sup>     |
| FS90 032          | 13 14 03.22   | -16 07 23.2    | 2850.3                         | 1             | 14.0           | ...            | S0                  |
| FS90 034          | 13 14 07.40   | -16 25 35.8    | 2688.2                         | 1             | 16.6           | ...            | dE <sup>a</sup>     |
| FS90 038          | 13 14 13.24   | -16 19 29.0    | 2564.9                         | 2             | 17.3           | 13.61±0.25     | E M32-type          |
| FS90 040          | 13 14 00.30   | -16 47 10.0    | 3044.5                         | 1             | 16.3           | ...            | SdIV                |
| FS90 041          | 13 14 16.70   | -16 33 24.0    | 2635.2                         | 2             | 18.8           | ...            | dE                  |
| FS90 042          | 13 14 17.36   | -16 26 19.5    | 2567.0                         | 1             | 15.9           | 12.48±0.19     | dE/dS0 <sup>a</sup> |
| FS90 045          | 13 14 20.00   | -15 53 01.0    | 2141.0                         | 3             | 18.9           | ...            | S or Im             |
| FS90 049          | 13 14 31.23   | -16 22 47.6    | 1465.2                         | 1             | 15.4           | ...            | ImIII               |
| FS90 050          | 13 14 34.86   | -16 29 28.9    | 2404.6                         | 1             | 15.8           | 12.12±0.12     | dE pec,N/BCDring    |
| FS90 051          | 13 14 35.84   | -16 34 50.4    | 2849.7                         | 1             | 16.5           | 13.57±0.29     | dE,N                |
| FS90 053          | 13 14 39.22   | -15 50 36.0    | 2324.3                         | 1             | 16.2           | 13.29±0.21     | BCD?                |
| FS90 054          | 13 14 39.40   | -16 10 04.0    | 2905.3                         | 1             | 16.7           | ...            | dE(Huge)            |
| FS90 057          | 13 14 43.54   | -16 22 54.9    | 2103.9                         | 1             | 18.8           | ...            | dE                  |
| FS90 058          | 13 14 43.61   | -15 51 34.4    | 2326.4                         | 1             | 18.8           | ...            | dE/Im               |
| FS90 063          | 13 14 49.82   | -16 58 24.2    | 2338.9                         | 1             | 15.2           | 11.73±0.12     | dS0                 |
| FS90 064          | 13 14 49.23   | -16 29 33.7    | 2147.4                         | 1             | 13.9           | 9.62±0.04      | SBa                 |
| FS90 068          | 13 14 59.37   | -16 35 25.1    | 1890.2                         | 1             | 13.0           | 8.67±0.08      | Sab(s)              |
| FS90 069          | 13 14 59.80   | -16 46 15.0    | 2567.6                         | 3             | 18.7           | ...            | dE                  |
| FS90 070          | 13 14 59.40   | -15 53 57.0    | 2626.6                         | 1             | 17.4           | ...            | dE                  |
| FS90 072          | 13 15 02.13   | -15 57 06.5    | 2234.2                         | 1             | 13.9           | 9.53±0.03      | S0                  |
| FS90 075          | 13 15 04.08   | -16 23 40.2    | 1913.4                         | 1             | 15.9           | 12.24±0.16     | dE <sup>a</sup>     |
| FS90 076          | 13 15 05.90   | -16 20 51.0    | 2702.0                         | 1             | 16.1           | 12.46±0.13     | d:E or E M32-type   |
| FS90 078          | 13 15 10.54   | -16 14 19.6    | 2741.3                         | 1             | 15.0           | 11.14±0.09     | E                   |
| FS90 079          | 13 15 12.71   | -16 29 57.1    | 2834.0                         | 1             | 16.1           | 12.88±0.17     | E                   |
| FS90 081          | 13 15 14.30   | -15 50 59.0    | 2232.9                         | 2             | 19.1           | ...            | dE                  |
| FS90 082          | 13 15 17.57   | -16 29 10.2    | 3495.8                         | 1             | 14.7           | 10.93±0.09     | S0/a                |
| FS90 083          | 13 15 21.60   | -16 36 08.0    | 2660.2                         | 1             | 17.4           | ...            | dE                  |
| FS90 084          | 13 15 23.97   | -16 23 07.9    | 2733.1                         | 1             | 11.9           | 7.71±0.02      | E                   |
| FS90 094          | 13 15 32.04   | -16 28 51.1    | 3168.9                         | 1             | 15.8           | 11.88±0.10     | d:E/S0              |
| FS90 095          | 13 15 32.40   | -16 38 12.0    | 2510.7                         | 1             | 18.8           | ...            | dE,N?               |
| FS90 096          | 13 15 32.70   | -16 50 35.0    | 3670.0                         | 3             | 18.5           | ...            | (interacting)?      |
| FS90 100          | 13 15 45.13   | -16 19 36.6    | 2227.6                         | 1             | 14.3           | 10.22±0.05     | E                   |
| FS90 102          | 13 15 48.52   | -16 31 08.0    | 1881.6                         | 1             | 13.7           | 9.42±0.03      | S0(cross)           |
| FS90 105          | 13 15 56.80   | -16 16 10.0    | 2847.6                         | 1             | 19.0           | ...            | dE,N                |
| FS90 107          | 13 15 59.30   | -16 23 49.8    | 2976.5                         | 1             | 13.8           | 9.43±0.15      | S0                  |
| FS90 108          | 13 15 59.90   | -16 10 32.0    | 2299.7                         | 1             | 17.4           | ...            | dE,N                |
| FS90 116          | 13 16 19.70   | -16 08 30.0    | 2612.9                         | 3             | 19.0           | ...            | dE,N                |
| FS90 117          | 13 16 23.11   | -16 08 11.4    | 2308.1                         | 1             | 15.8           | 11.86±0.12     | d:E,N               |
| FS90 121          | 13 16 31.30   | -16 40 40.0    | 2191.0                         | 1             | 18.6           | ...            | dE/Im               |

Table 1 (cont'd)

| Galaxy Identifier       | RA<br>(J2000) | DEC<br>(J2000) | $cz$<br>( $\text{km s}^{-1}$ ) | FS90<br>Memb. | $B_T$<br>(mag) | $K_T$<br>(mag) | Morphology      |
|-------------------------|---------------|----------------|--------------------------------|---------------|----------------|----------------|-----------------|
| (1)                     | (2)           | (3)            | (4)                            | (5)           | (6)            | (7)            | (8)             |
| FS90 123                | 13 16 35.62   | -16 26 05.7    | 2537.9                         | 1             | 18.3           | ...            | dE,N?           |
| FS90 127                | 13 16 39.40   | -16 57 03.0    | 3089.3                         | 1             | 18.6           | ...            | dE              |
| FS90 133                | 13 16 55.43   | -16 26 32.2    | 2589.1                         | 2             | 18.6           | ...            | dE,N            |
| FS90 134                | 13 16 56.23   | -16 35 34.7    | 2051.0                         | 1             | 15.1           | ...            | Sm(interacting) |
| FS90 135                | 13 16 54.40   | -16 03 18.0    | 3242.2                         | 1             | 18.6           | ...            | dE,N            |
| FS90 137                | 13 16 58.49   | -16 38 05.5    | 1657.7                         | 1             | 11.5           | ...            | Sb(s)I-II(int.) |
| FS90 138                | 13 17 03.10   | -16 35 39.0    | 2277.0                         | 2             | 19.0           | ...            | dE,N            |
| FS90 141                | 13 17 06.13   | -16 15 07.9    | 2563.3                         | 1             | 13.5           | ...            | Sd(on edge)     |
| FS90 144                | 13 17 10.80   | -16 13 46.7    | 2511.0                         | 1             | 14.8           | 11.27±0.06     | E? + dE?        |
| FS90 146                | 13 17 14.00   | -16 59 59.0    | 2538.1                         | 3             | 19.1           | ...            | S or dE,N       |
| FS90 151                | 13 17 32.00   | -15 52 51.0    | 2165.0                         | 2             | 19.0           | ...            | dE              |
| FS90 153                | 13 17 36.38   | -16 32 25.4    | 2900.2                         | 1             | 15.4           | 11.73±0.11     | d:S0            |
| FS90 155                | 13 17 40.90   | -15 44 35.0    | 2922.0                         | 1             | 17.4           | ...            | Sm              |
| FS90 158                | 13 18 09.04   | -16 58 15.6    | 2784.2                         | 3             | 16.9           | 13.15±0.16     | dS0 or S0       |
| FS90 161                | 13 18 17.80   | -16 38 25.0    | 2153.0                         | 1             | 18.9           | ...            | dE              |
| 2MASX J13085477-1636106 | 13 08 54.79   | -16 36 10.4    | 2585.8                         | ...           | 16.37          | 12.97±0.15     | ...             |
| 2MASX J13094408-1636077 | 13 09 44.07   | -16 36 07.6    | 2582.0                         | ...           | 13.87          | 9.75±0.03      | S0+             |
| 2MASX J13091671-1653115 | 13 09 16.74   | -16 53 11.8    | 2420.9                         | ...           | 16.40          | 12.83±0.19     | ...             |
| 2MASX J13095347-1631018 | 13 09 51.70   | -16 30 55.7    | 2376.0                         | ...           | ...            | 11.52±0.11     | S0-             |
| 2MASX J13100952-1616458 | 13 10 09.52   | -16 16 45.6    | 2226.0                         | ...           | 17.23          | 12.34±0.13     | ...             |
| 2MASX J13102493-1655578 | 13 10 24.96   | -16 55 57.5    | 2423.9                         | ...           | 13.94          | 10.11±0.09     | ...             |
| 2MASX J13114576-1915421 | 13 11 45.77   | -19 15 42.3    | 2751.3                         | ...           | ...            | 9.44±0.04      | (R')SB(r)a      |
| 2MASX J13114703-1847312 | 13 11 47.04   | -18 47 31.3    | 2532.7                         | ...           | 15.67          | 12.93±0.12     | S               |
| 2MASX J13115849-1644541 | 13 11 58.49   | -16 44 54.1    | 2906.9                         | ...           | 15.29          | 11.96±0.09     | ...             |
| 2MASX J13123543-1732326 | 13 12 35.43   | -17 32 32.7    | 2760.0                         | ...           | 13.14          | 8.85±0.03      | SAB(s)c         |
| 2MASX J13133433-1525554 | 13 13 34.34   | -15 25 55.2    | 2503.0                         | ...           | 13.71          | 10.85±0.09     | SAB(s)dm        |
| 2MASX J13143041-1732009 | 13 14 30.42   | -17 32 00.9    | 2517.1                         | ...           | 15.23          | 11.54±0.09     | ...             |
| 2MASX J13151278-1758006 | 13 15 12.80   | -17 58 00.4    | 3006.4                         | ...           | 14.61          | 12.32±0.15     | SAB(s)d         |
| 2MASX J13153736-1452209 | 13 15 37.38   | -14 52 21.1    | 2710.0                         | ...           | ...            | 11.24±0.08     | ...             |
| 2MASX J13164875-1620397 | 13 16 48.75   | -16 20 39.7    | 2619.1                         | ...           | 15.45          | 11.60±0.12     | ...             |
| 2MASX J13165533-1756417 | 13 16 55.35   | -17 56 42.0    | 2529.7                         | ...           | 15.26          | 11.94±0.09     | S0-a            |
| 2MASX J13171239-1715162 | 13 17 12.40   | -17 15 16.1    | 2514.1                         | ...           | 14.24          | 10.24±0.04     | SAB(r)bc        |
| 2MASX J13182685-1545599 | 13 18 26.85   | -15 46 00.5    | 2853.0                         | ...           | ...            | 11.57±0.08     | Sb              |
| 2MASX J13183034-1436319 | 13 18 30.35   | -14 36 32.0    | 2889.0                         | ...           | ...            | 10.48±0.06     | SA(r)c pec?     |
| 2MASX J13184125-1904476 | 13 18 41.26   | -19 04 47.7    | 2718.3                         | ...           | 15.77          | 12.06±0.10     | Sa              |
| 2MASX J13185909-1835167 | 13 18 59.09   | -18 35 16.7    | 2578.0                         | ...           | 14.14          | 10.12±0.04     | SA0-            |
| 2MASX J13191752-1509252 | 13 19 17.52   | -15 09 25.3    | 2832.0                         | ...           | ...            | 10.85±0.06     | ...             |
| 2MASX J13192062-1450402 | 13 19 20.65   | -14 50 40.3    | 2744.0                         | ...           | 13.14          | 9.16±0.03      | SB(s)c? sp      |
| 2MASX J13192221-1509232 | 13 19 22.22   | -15 09 23.5    | 2832.0                         | ...           | ...            | 13.16±0.11     | ...             |
| 2MASX J13201698-1448455 | 13 20 17.01   | -14 48 46.2    | 2853.0                         | ...           | ...            | 11.33±0.06     | ...             |
| 2MASXi J1320185-163215  | 13 20 18.50   | -16 32 12.0    | 2285.0                         | ...           | 14.44          | 11.13±0.06     | ...             |
| 6dF j1311150-180610     | 13 11 15.03   | -18 06 09.6    | 2727.0                         | ...           | 16.16          | 13.80±0.23     | ...             |
| 6dF j1313501-173048     | 13 13 50.08   | -17 30 47.8    | 2223.3                         | ...           | 16.84          | ...            | ...             |
| GEMS_N5044_5            | 13 05 37.27   | -15 46 58.5    | 2912                           | ...           | ...            | ...            | ...             |
| GEMS_N5044_14           | 13 08 05.02   | -14 44 53.3    | 2599                           | ...           | ...            | ...            | ...             |
| GEMS_N5044_7            | 13 10 59.34   | -15 20 44.3    | 2828                           | ...           | 17.68          | 13.62±0.23     | ...             |
| GEMS_N5044_18           | 13 11 36.13   | -14 40 40.1    | 2472                           | ...           | ...            | ...            | ...             |
| GEMS_N5044_1            | 13 14 09.93   | -16 41 41.6    | 3074                           | ...           | ...            | ...            | ...             |
| PGC 045257              | 13 05 15.60   | -16 53 19.0    | 2842                           | ...           | 15.05          | ...            | SAB(s)m         |
| PGC 046242              | 13 16 52.70   | -17 53 54.4    | 2580                           | ...           | 16.96          | ...            | Dwarf           |
| PGC 046402              | 13 18 56.50   | -17 38 06.0    | 2495                           | ...           | 16.31          | ...            | SAB(rs)m        |
| PGC 046494              | 13 19 54.83   | -17 18 55.8    | 2689                           | ...           | 15.54          | ...            | SB(s)dm         |
| HIPASS J1312-15         | 13 12 36.20   | -15 52 43.0    | 2953                           | ...           | ...            | ...            | ...             |
| HIPASS J1320-14         | 13 20 18.80   | -14 27 42.0    | 2750                           | ...           | ...            | ...            | ...             |
| FGC1563                 | 13 08 13.90   | -16 14 21.0    | 2790                           | ...           | 16.4           | 13.23±0.65     | Sdm             |

Note. — Columns are as follows: (1) Galaxy Identifier (2) Right ascension (J2000), (3) Declination (J2000), (4) Recession Velocity, (5) FS90 membership classification, where 1,2 and 3 represent definite, likely and possible members respectively, (6) B-band magnitude, (7) K-band magnitude and error, (8) Morphological type. For FS90 galaxies we adopt their morphological classification, except where morphologies have been modified by Cellone & Buzzoni (2005; marked with <sup>a</sup>). For all other galaxies morphologies are adopted from NED.

#### 4.1 Comparison with FS90

FS90 used morphological criteria to arrive at their original membership classification (e.g. low-luminosity spiral galaxies are likely to be background objects). Since we have obtained recession velocities for 103 of their 162 NGC 5044 group galaxies we are able to re-evaluate their original group membership. FS90 organised their observations into three different membership classes designated 1 (definite members), 2 (likely members) and 3 (possible members).

Our spectroscopic sample includes 60, 14 and 29 class 1, 2 and 3 galaxies respectively. Confirmed NGC 5044 group members and their FS90 classifications are shown in Table 1. Non-members, their velocities and FS90 classifications are given in Table 2. Of class 1 galaxies we find 55 of the 60 to be genuine group members,  $\sim 92$  percent, indicating that class 1 galaxies in the FS90 catalogue are generally reliable group member galaxies. The fractions of genuine group member class 2 and 3 galaxies fall, as one might expect based on their increasing uncertainty in group membership, and we confirm 7 class 2 and 9 class 3 galaxies as bona fide group members (50 and  $\sim 31$  percent respectively). We note that the NGC 5044 group is the most distant considered by FS90, and so it is perhaps not surprising that the classification of galaxies is somewhat unreliable given the difficulty in morphologically classifying faint galaxies.

Fig. 6 shows a comparison of the B-band luminosity functions (LF) between our confirmed group sample and the complete FS90 sample. The largest difference between the two comes at faint magnitudes where our spectral observations become significantly incomplete and FS90 likely includes a significant number of faint class 3 membership galaxies, of which our observations suggest only one-third are actually group members.

We adopt a Monte Carlo approach to correct the LFs shown in Fig. 6 for our own incompleteness and contamination present in the FS90 sample. Confirmed group member galaxies are always included in the analysis, however there are 59 dwarf galaxies in the FS90 sample with no recession velocity information. We therefore sample these remaining FS90 dwarf galaxies based on the fractions of class 1, 2 and 3 included in our confirmed group sample (i.e. 92, 50 and 31 percent of each respective membership class are included in the Monte Carlo group each iteration). This provides a more accurate estimate of the luminosity function and allows us to examine the effect of contamination on the FS90 sample.

Fig. 6 shows that our spectroscopic sample is in excellent agreement with the FS90 sample for  $M_B < -15$ , where the FS90 sample is greater than 90 percent complete, and implies a flat luminosity function. In the region  $-15 < M_B < -14$  our spectroscopic sample begins to deviate from the FS90 sample, however our Monte Carlo corrections show that the majority of this is due to the inclusion of outliers in the FS90 sample, rather than incompleteness in our data. Below  $M_B > -14$  the LF shows tentative evidence for an upturn, however our sample is significantly incomplete in this magnitude range so we abstain from drawing any further conclusions.

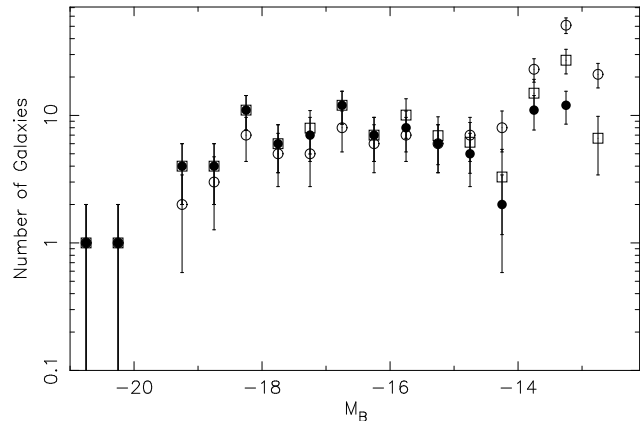


**Figure 6.** B-band luminosity function for the NGC 5044 group. Open circles represent the luminosity function of the FS90 sample, while filled circles represent our spectroscopically confirmed group member sample. Open squares show the results of including additional galaxies from the FS90 sample based on their likelihood of group membership (see §4.1). Galaxies are binned at 0.5 magnitude intervals and Poisson errors are shown. Note that points may overlap.

## 5 GLOBAL PROPERTIES

A vital step in establishing the role that groups play in the evolution of galaxies is establishing their place between clusters and the field. Are groups simply low-mass clusters, or do their member galaxies exhibit unique signs of formation and evolution? In order to assess this we first need to establish the relation of the NGC 5044 group to other groups and clusters.

The dynamical properties of the NGC 5044 group are summarised in Table 3, which shows the mean velocity, velocity dispersion,  $R_{500}$  radius<sup>1</sup>, dynamical mass and crossing time we derive using the formulae in Appendix A. For comparison, we also show similar measurements from the literature.

While we have more than tripled the number of group members included relative to previous studies, our results for the mean velocity, velocity dispersion,  $R_{500}$  radius, mass and crossing time are all consistent within errors. We find the group to be massive, nearly  $10^{14} M_{\odot}$  in total mass, which combined with the short crossing time leads us to the same conclusions of B06 that the NGC 5044 group is a classically massive, dynamically mature group.

### 5.1 Dynamical state

Addressing the dynamical state of the NGC 5044 group is key in our goal of establishing its evolutionary history. In particular, the brightest group galaxy (NGC 5044) is known to have a peculiar velocity of  $\sim 150 \text{ km s}^{-1}$  with respect to the mean group velocity (Cellone & Buzzoni 2005; B06), which could be indicative of non-equilibrium due to recent mergers. The peculiar velocity found for NGC 5044, scaled by the group’s velocity dispersion, is  $0.45\sigma_v$ , and within the range typically found for relaxed groups and clusters (e.g. Oegerle

<sup>1</sup> The  $R_{500}$  radius is defined as the radius at which the projected density reaches 500 times the critical density.

**Table 3.** NGC 5044 group dynamical properties compared with available literature values.

| Source                   | N   | $\bar{v}$<br>( $\text{km s}^{-1}$ ) | $\sigma_v$<br>( $\text{km s}^{-1}$ ) | $r_{500}$<br>(Mpc) | $M_v$<br>( $10^{13} M_\odot$ ) | $t_c$<br>( $H_0^{-1}$ ) |
|--------------------------|-----|-------------------------------------|--------------------------------------|--------------------|--------------------------------|-------------------------|
| (1)                      | (2) | (3)                                 | (4)                                  | (5)                | (6)                            | (7)                     |
| This Work                | 111 | 2577±33                             | 331±26                               | 0.53±0.05          | 9.2±1.6                        | 0.03±0.004              |
| B06                      | 32  | 2548±14                             | 402±53                               | 0.55±0.07          | 6.9±1.9                        | 0.01±0.004              |
| Cellone & Buzzoni (2005) | 26  | 2461±84                             | 431                                  | ...                | ...                            | ...                     |
| Osmond & Ponman (2004)   | 18  | 2518±100                            | 426±74                               | 0.62±0.08          | ...                            | ...                     |

Notes. Columns are as follows: (1) Source. (2) Number of group members included in the calculated values. (3) Mean recession velocity and  $\sigma/\sqrt{N}$  error. (4) Velocity dispersion and  $1\sigma$  error (when available). (5)  $r_{500}$  radius. (6) Crossing time.

**Table 2.** Confirmed non-members and possible stars from the Ferguson & Sandage (1990) NGC 5044 Catalogue

| FS90<br>(#)           | RA<br>(J2000) | DEC<br>(J2000) | $cz$<br>( $\text{km s}^{-1}$ ) | FS90<br>Memb. |
|-----------------------|---------------|----------------|--------------------------------|---------------|
| (1)                   | (2)           | (3)            | (4)                            | (5)           |
| 002                   | 13 12 18.60   | -16 47 40.0    | 69871.0                        | 3             |
| 004                   | 13 12 36.50   | -16 13 52.0    | 4943.4                         | 3             |
| 010                   | 13 13 04.89   | -16 15 46.9    | 12811.0                        | 3             |
| 021                   | 13 13 39.60   | -16 01 47.0    | 17082.3                        | 3             |
| 023                   | 13 13 46.62   | -16 20 07.9    | 103570.2                       | 2             |
| 028                   | 13 13 55.90   | -16 35 49.0    | 9054.7                         | 1             |
| 033                   | 13 14 05.10   | -15 55 42.0    | 13667.6                        | 3             |
| 037                   | 13 14 12.30   | -16 40 16.0    | 29078.4                        | 3             |
| 039                   | 13 14 13.05   | -16 11 14.9    | 28842.1                        | 3             |
| 046                   | 13 14 25.59   | -16 17 50.9    | 17122.0                        | 1             |
| 059                   | 13 14 43.60   | -15 44 48.0    | 42551.5                        | 3             |
| 088                   | 13 15 26.80   | -15 55 22.0    | 11048.0                        | 3             |
| 090                   | 13 15 27.80   | -16 11 41.0    | 28856.0                        | 2             |
| 099                   | 13 15 42.70   | -16 33 01.0    | 98838.7                        | 3             |
| 109                   | 13 16 08.00   | -16 59 49.0    | 5385.9                         | 1             |
| 110                   | 13 16 06.79   | -16 08 40.4    | 221397.9                       | 3             |
| 115                   | 13 16 19.68   | -16 40 13.7    | 5436.6                         | 3             |
| 124                   | 13 16 35.80   | -15 57 08.0    | 157159.7                       | 2             |
| 130                   | 13 16 47.50   | -16 28 04.0    | 17422.1                        | 1             |
| 136                   | 13 16 56.68   | -16 18 44.7    | 29325.4                        | 3             |
| 143                   | 13 17 09.30   | -16 51 18.0    | 84111.4                        | 3             |
| 152                   | 13 17 34.30   | -16 10 58.0    | 13925.5                        | 2             |
| 157                   | 13 17 49.40   | -16 53 39.0    | 19548.4                        | 3             |
| 159                   | 13 18 12.39   | -15 41 25.8    | 11381.8                        | 2             |
| 160                   | 13 18 11.50   | -16 06 57.0    | 41112.6                        | 3             |
| <i>possible stars</i> |               |                |                                |               |
| 008                   | 13 12 57.30   | -16 33 10.0    | 37.0                           | 3             |
| 014                   | 13 13 12.20   | -16 28 03.0    | -18.1                          | 3             |
| 026                   | 13 13 54.70   | -16 27 10.0    | -33.1                          | 2             |
| 036                   | 13 14 12.30   | -16 28 58.0    | 15.4                           | 2             |
| 052                   | 13 14 36.80   | -16 07 56.0    | -71.6                          | 3             |
| 061                   | 13 14 47.90   | -16 17 51.0    | -49.7                          | 3             |
| 118                   | 13 16 26.00   | -17 03 19.0    | 87.2                           | 3             |

Notes. Columns are as follows: (1) FS90 galaxy identifier, (2) Right ascension, (3) Declination, (4) Measured recession velocity, (5) FS90 membership classification, where 1,2 and 3 represent definite, likely and possible members respectively.

& Hill 2001; B06; Hwang & Lee 2007). Peculiar brightest group and cluster galaxy (BGG/BCG) velocities are therefore not in and of themselves indicative of groups out of dynamical equilibrium.

To further assess the dynamical state of the NGC 5044 group we examine both the characteristics of line-of-sight (LOS) velocities and dynamical measurements such as cross-

ing time. Fig. 7 shows the LOS velocity distribution for our group sample with the best fit Gaussian overlaid. Fitting a fourth-order Gauss-Hermite expansion to our LOS velocities (e.g. Zabludoff, Franx & Geller 1993) we find negligible values for the  $h_3$  and  $h_4$  coefficients, measurements of the distribution skewness and kurtosis. The normal distribution of LOS velocities suggests that the group is relaxed and well mixed, as  $h_3$  and  $h_4$  are generally indicative of substructure or strong orbital anisotropies in the group velocities (e.g. Merritt 1988; Zabludoff *et al.* 1993).

The crossing time of a group can also be used as a indication of a group’s virialization, where crossing times  $> 0.09 H_0^{-1}$  are usually indicative of groups whose galaxy orbits have not had sufficient time to circularise in the group potential (Nolthenius & White 1987). The short crossing time found for the NGC 5044 group ( $t_c = 0.03 \pm 0.004 H_0^{-1}$ ,  $\sim 0.4$  Gyrs) therefore suggests that it is most likely virialised and consistent with the low kurtosis we find for the velocity distribution, discussed above.

The use of crossing time as an indicator of virialization can be somewhat questionable in groups, and studies examining very small groups ( $N_{gal} \sim 5 - 10$ ) have found that using  $t_c$  as the sole indicator of virialization can lead to the inclusion of up to 20 percent spurious associations (see e.g. Diaferio *et al.* 1993; Niemi *et al.* 2007). However this discrepancy is primarily a concern for galaxies which are only questionably bound. A comparison of the NGC 5044 group to the virial parameters discussed in Niemi *et al.* (2007) suggests that groups of order the NGC 5044 group mass are bound with greater than 99 percent probability and that the crossing time is a useful indicator in assessing dynamical status.

The availability of XMM X-ray observations for the NGC 5044 group (T. Ponman, private communication) means that we have an additional and independent measure for the group centre of mass. Poole *et al.* (2006) have shown that an offset in the X-ray peak from the centroid of emission is an excellent indicator of dynamical equilibrium in clusters as sub-cluster mergers can cause the X-ray peak to “slosh” with respect to the centroid. Using an XMM mosaic, we calculate the peak-centroid displacement for the NGC 5044 group, finding a nominal offset of  $\sim 0.003 R_{500}$ , which is within the range of relaxed clusters in the Poole *et al.* (2006) simulations. We do note, however, that this test is sensitive only to offsets in the plane of the sky, and so we are unable to rule out significant displacements of the X-ray peak along the line of sight.

From the above indicators we therefore conclude that the NGC 5044 group is in equilibrium and virialized.

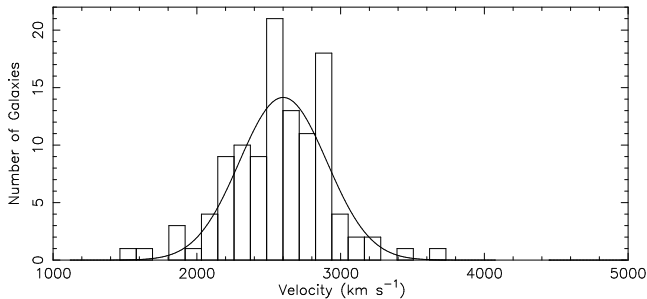


**Figure 7.** Histogram of the velocities measured in our group sample. The solid line represents the best fit fourth order Gauss-Hermite series to the velocity data.

## 5.2 Substructure

Based on the paradigm of hierarchical structure formation, conglomerations of galaxies such as clusters and large groups are formed via the successive infall of smaller structures. Substructures are found in anywhere from 30 to 70 percent of optically observed clusters (West 1988; Girardi *et al.* 1997; Burgett *et al.* 2004; Ramella *et al.* 2007), providing considerable evidence in support of this merging scenario. While the NGC 5044 group is considerably smaller than rich clusters typically analysed we still expect it to have evolved via similar hierarchical mechanisms, and so a search for dynamical substructures is relevant.

Here we adopt the Dressler-Shectman  $\Delta$  statistic (Dressler & Shectman 1998) as a means for measuring the three-dimensional (space-velocity) substructure present in our sample. This statistic, while originally used for measurement of substructure in clusters, has been shown to be effective at identifying dynamical substructures even at smaller, group scales (Pinkney *et al.* 1996).

Calculation of the  $\Delta$  statistic involves the summation of local velocity anisotropy,  $\delta$ , for each galaxy in the group, defined as

$$\delta^2 = \left( \frac{N_{\text{nn}} + 1}{\sigma^2} \right) [(\bar{v}_{\text{local}} - \bar{v}_{\text{group}})^2 - (\sigma_{\text{local}} - \sigma)^2] \quad (1)$$

where  $N_{\text{nn}}$  is the number of nearest neighbours over which the local recession velocity ( $\bar{v}_{\text{local}}$ ) and velocity dispersion ( $\sigma_{\text{local}}$ ) are calculated. Here we adopt  $N_{\text{nn}} = \sqrt{N}$ , following Pinkney *et al.* (1996). The test statistic  $\Delta$  is larger for increasing levels of substructure in the group.

In order to provide a normalisation for this statistic, and therefore a means of measuring its significance, we perform 1000 Monte Carlo simulations of our data, randomly shuffling the velocities in the group and re-calculating the  $\Delta$  statistic. This allows us to calculate the probability that our measured  $\Delta$  can be obtained from a random distribution of recession velocities.

It is important to note that there are two insensitivities of the  $\Delta$  statistic that must also be considered. The first is related to the  $\Delta$  statistic's inability to detect superimposed substructures, mentioned by Dressler & Shectman (1988). A second caveat is that the  $\Delta$  statistic is insensitive to equal mass mergers occurring in the plane of the sky (i.e. similar mean velocity and dispersion), as discussed by Pinkney *et al.* (1996).

We find suggestions of substructure in the NGC 5044 group, with the group's  $\Delta$  value significant at greater than

the 99.9 percent level. It is possible that high  $\Delta$  values can be obtained via rotation or velocity gradients across the group. Based on this, we have examined our velocity data for any signs of rotation, however we find no evidence for bulk rotation with  $v_{\text{rot}} \sim 53 \pm 49 \text{ km s}^{-1}$ .

To visually search for merging sub-groups that could be responsible for the large  $\Delta$  value, in Fig. 8 we show a bubble plot for the NGC 5044 group. Here, each galaxy is represented with a circle whose radius is scaled as  $e^\delta$  (where  $\delta$  is taken from Eq. 1). As is evident from this figure, there is a significant sub-clump of galaxies in the north-east outskirts of the group, which is responsible for the high  $\Delta$  value. Removing these galaxies and re-running the substructure test results in the group's  $\Delta$  value being significant at only the 70 percent level.

## 5.3 Number density profile

Hierarchical formation in the context of the  $\Lambda$ CDM paradigm makes particular statistical predictions regarding the shape of resulting density profiles. These predictions are primarily motivated by numerical simulations and suggest that halo profiles are well described by a combination of power laws growing progressively steeper with increasing radius (Dubinski & Carlberg 1991; Navarro, Frenk & White 1995, 1996, 1997). Such exponential profiles have been found to be applicable across a range of groups and clusters (e.g. Carlberg *et al.* 1997; Carlberg, Yee & Ellingson 1997; Biviano & Girardi 2003).

The average projected number density of galaxies,  $\Sigma_N$ , can be represented as a projection of the volume density  $\nu(r)$  via an Abel integral where

$$\Sigma_N(R) = 2 \int_R^\infty \nu(r) \frac{r}{\sqrt{r^2 - R^2}} dr. \quad (2)$$

Here we adopt a general form of the volume density

$$\nu(r) = \frac{A}{r(r + a_v)^p}, \quad (3)$$

where  $a_v$  is the radius of the transition between the inner and outer profile slopes. Different outer slopes of the profiles are obtained for a fixed value of  $p$ , and adopting  $p = 2$  or 3 gives an NFW (Navarro, Frenk & White 1995, 1996, 1997) or Hernquist (Hernquist 1990) profile respectively. In Fig. 9 we show the binned surface density profiles calculated for each of the three data sets (either NED, 6dFGS or AAOmega), where the 6dFGS and AAOmega bins have been corrected for their known incomplete spatial coverage. As a rough correction to facilitate fitting a mean density profile we have scaled the data to match in density between 0.2 and 0.6 Mpc, applying the derived offset to the remaining bins.

The profiles fit to this corrected data are shown with the solid and dashed lines (NFW and Hernquist profiles) in Fig. 9, where bins containing a single galaxy have been excluded from the fitting process. Both fits are reasonable, however the NFW profile provides a statistically better fit. The scale radius for the best fit NFW profile is  $a_v = 0.26 \pm 0.02$ , consistent with the CNOC cluster profile fits of Carlberg *et al.* (1997). For the remainder of relevant analyses we will consider only the best fit NFW profile.

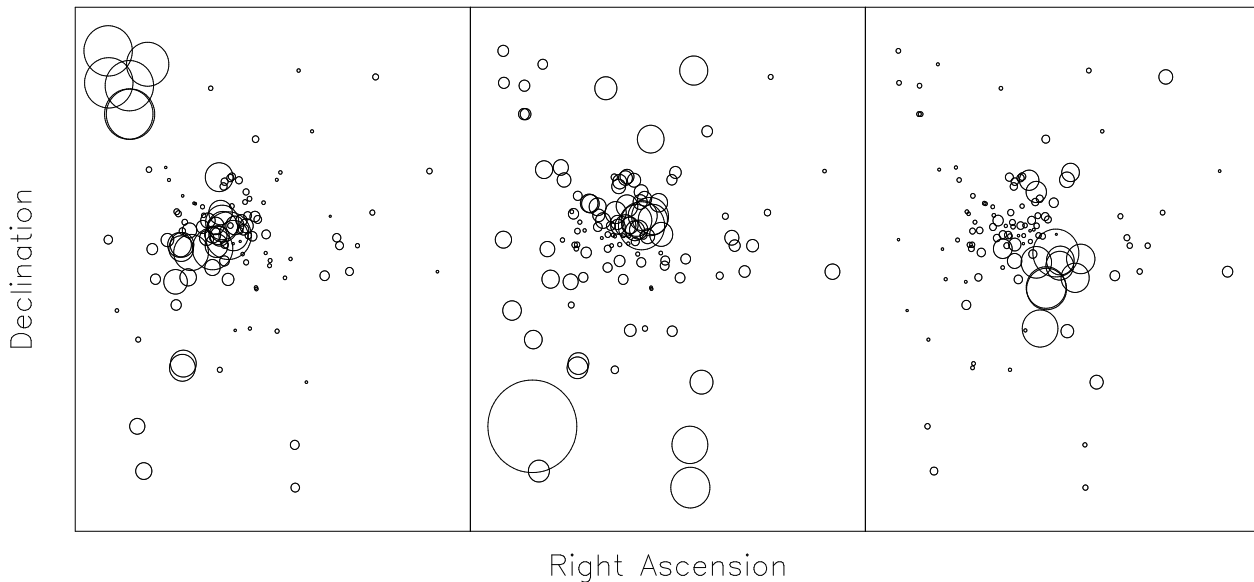


**Figure 8.** Bubble diagram for the Dressler-Shectman substructure test. Each circle represents a galaxy in the NGC 5044 group with sizes scaled by  $e^\delta$  (see text). The left panel shows galaxies scaled by their observed  $\delta$  while the centre and right panels show the maximal and median substructure results from our Monte Carlo simulations of the data. Orientation and area displayed in each panel are the same as in Fig. 5.

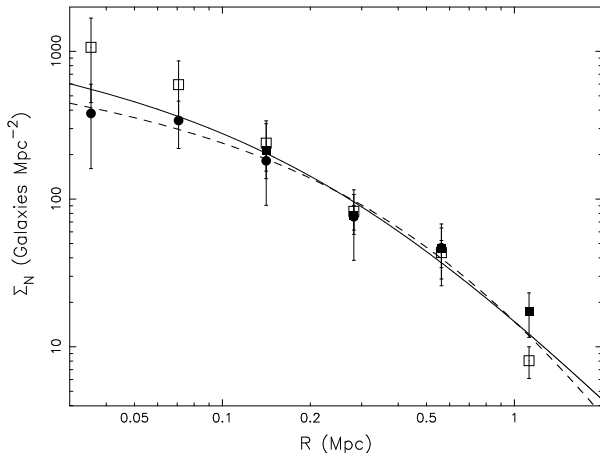


**Figure 9.** Average projected number density as a function of radius. Open squares, filled circles and filled squares represent NED, AAOmega and 6dFGS data respectively. Data are scaled to match in number density at radii between 0.1 and 0.6 Mpc (see §5.3). Note that as a result of this scaling symbols overlap. The solid and dashed lines represent the best fit NFW and Hernquist profiles.

#### 5.4 Velocity dispersion profile

The underlying mass distribution of a group or cluster is related to the volume density and velocity dispersion profiles via the Jeans equations. By measuring the observed density and velocity distributions, one can infer properties of the group mass distribution. This analysis is often applied to group and cluster systems where galaxies can be treated as tracer particles, with the caveat that interpretation using the Jeans equations is only appropriate for systems in equilibrium.

The velocity dispersion profiles of clusters are generally found to be falling with radius (e.g. Carlberg, Yee & Elling-

son 1997; Carlberg *et al.* 1997; Girardi *et al.* 1998; Biviano & Girardi 2003; Biviano & Katgert 2004) and indicative of centrally concentrated mass distributions. Group studies measuring velocity dispersion profiles are generally in good agreement, finding either falling or roughly flat profiles with radius (e.g. Zabludoff & Mulchaey 1998; B06). However, there is some evidence that the velocity dispersion is actually smoothly rising with radius (Carlberg *et al.* 2001), suggesting that galaxies are concentrated with respect to the dark matter distribution due to contraction within the halo (e.g. by dynamical friction).

The velocity dispersion at a given radius is calculated here in a similar fashion to the number density, using the projection of the radial velocity dispersion and number density such that

$$\sigma_p^2(R) = \frac{1}{\Sigma_N(R)} \int_R^\infty \nu \sigma_r^2 \left(1 - \beta \frac{R^2}{r^2}\right) \frac{r}{\sqrt{r^2 - R^2}} dr, \quad (4)$$

where  $\beta = 1 - \sigma_\theta^2/\sigma_r^2$  is the velocity anisotropy parameter. We have adopted a simple form of the radial velocity dispersion used by Carlberg *et al.* (1997) defined as

$$\sigma_r^2(r) = \frac{B}{b+r}. \quad (5)$$

where  $B$  and  $b$  are free parameters in our fit.

In Fig. 10 we show the velocity dispersion profile derived for our data, with best fit velocity dispersion profiles for  $\beta = 1, \frac{1}{2}$  and 0 (purely radial, marginally isotropic, and isotropic orbits). Bins contain 10 galaxies each and velocity dispersions have been calculated using the gapper algorithm (Beers *et al.* 1990; Eq. A4). As expected for a relaxed group, we find the velocity dispersion falling with radius regardless of our allowed values of  $\beta$ , implying that the group mass is centrally concentrated and in agreement with the profile found by B06 for their stacked GEMS groups.

There is some suggestion of fluctuation in the veloc-

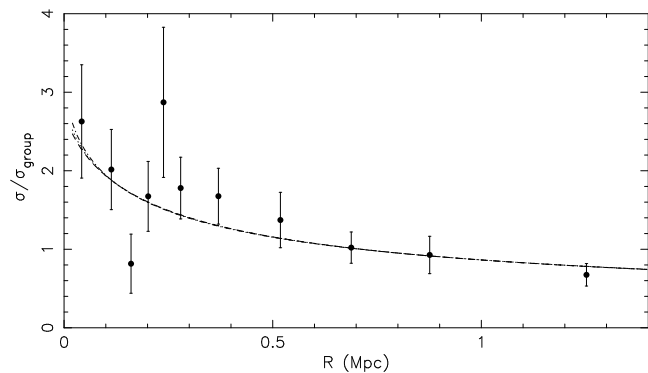


**Figure 10.** Velocity dispersion profile of the NGC 5044 group. NGC 5044 is assumed to be the centre of the group. Bins contain 10 galaxies each and  $1\sigma$  jackknife errors are shown. Best fit profiles for  $\beta = 1, \frac{1}{2}$  and 0 are overlaid (lines overlap).

**Table 4.** Comparison of mass estimates from the literature.

| Source<br>(1)                      | Method<br>(2) | $M$ ( $10^{13}M_{\odot}$ )<br>(3) | $R$ (Mpc)<br>(4) |
|------------------------------------|---------------|-----------------------------------|------------------|
| This Work                          | Dynamical     | $9.2 \pm 1.6$                     | ...              |
| Brough <i>et al.</i> (2006)        | Dynamical     | $6.9 \pm 1.9$                     | ...              |
| David <i>et al.</i> (1994)         | X-ray         | 1.6                               | $< 0.18$         |
| Betoya-Nonesa <i>et al.</i> (2006) | X-ray         | 1.6                               | $< 0.18$         |
| Betoya-Nonesa <i>et al.</i> (2006) | X-ray         | 5.1                               | $< 0.58$         |

ity dispersion profile between 100 and 200 kpc (also seen in Fig. 4), however due to our relatively low numbers its significance is unclear. Fluctuations in the velocity dispersion profile are commonly observed in clusters (see e.g. den Hartog & Katgert 1996) and studies which allow the orbital anisotropy parameter,  $\beta$ , to vary find that these fluctuating profiles can be reasonably fit by a varying orbital distribution with radius (see e.g. Biviano & Katgert 2004; Hwang & Lee 2007). These velocity dispersion variations can also be produced if there are multiple sub-populations in the group, either on uniquely different orbits (e.g. radial or tangential) or offset from the assumed centre of the group.

## 5.5 Mass estimates

Table 4 shows a comparison of mass estimates for the NGC 5044 group in the literature, derived both dynamically and from X-rays. As this table shows, there are a variety of estimates for the NGC 5044 group mass from  $\sim 10^{13}$  to  $10^{14} M_{\odot}$ . Given this variation, and our attempt to compare the NGC 5044 group with other groups and clusters, we will briefly examine the reliability and consistency of these mass estimates.

For this comparison we have built a sample of groups and clusters using two separate data sets. The first is the 15 Southern GEMS groups studied by B06, which contains groups in the range  $12.3 < \log M_{\odot} < 13.8$ . B06 have calculated the dynamical properties of these groups (i.e. virial mass, radius etc.) and the X-ray properties of the groups have been presented by Osmond & Ponman (2004).

The second data set consists of 38 clusters from the *Advanced Satellite for Cosmology and Astrophysics* (ASCA) Cluster Catalogue of Horner (2001; ACC). The velocity dis-

persion and virial mass measurements for these clusters have been adopted from Girardi *et al.* (1998), and only those clusters with  $>30$  confirmed members are included in this analysis.

In order to compare the X-ray and dynamical masses for a number of sources, we first need normalise them to a standard mass scale. For dynamical masses this normalisation is not straight forward. Masses for the GEMS and ACC samples are both calculated as virial masses, which implies a density contrast of  $\delta_{vir} = 18\pi^2 \approx 178$  for an  $\Omega_0 = 1$  universe (Bryan & Norman 1998). However there is no implicit radius assumption in these calculations, so scaling these masses to a different density contrast (e.g.  $\delta = 200$ ) is difficult.

We calculate X-ray masses to a similar density contrast as the dynamical estimates. This has been done using the  $\beta$ -model fit parameters to calculate the group mass in terms of density contrast and X-ray temperature (Horner, Mushotzky & Scharf 1999) such that

$$M(\delta, \beta, T_X) = 1.1 \times 10^{15} \delta^{-1/2} \beta^{-3/2} \left( \frac{T_X}{\text{keV}} \right)^{3/2} \times \left( 1 - 0.01 \frac{\delta r_c^2}{\beta T_X} \right)^{3/2} h^{-1} M_{\odot}. \quad (6)$$

In this case, we adopt  $\delta = 178$  and use the  $\beta$ -model fits from Osmond & Ponman (2004) for the GEMS groups and Fukazawa (1997) for the ACC cluster sample.

In Fig. 11 we show the comparison of dynamical masses and re-calculated X-ray masses. This comparison shows a systematic offset between X-ray and dynamical masses, however the two estimates scale almost linearly. For the NGC 5044 group, the mass we calculate using Eq. 6 is consistent with that of Betoya-Nonesa *et al.* (2006), i.e.  $\sim 5.1 \times 10^{13} M_{\odot}$ , while our dynamical mass is consistent with the general group and cluster trend. So, while the dynamical and X-ray masses for this group disagree, their disagreement is consistent with the systematic offset present between the two methods used.

## 5.6 Group scaling relations

In self-similar models of group and cluster formation the amount of gas present in a halo is directly related to the depth of the potential well, leading to correlations of X-ray luminosity with both gas temperature and velocity dispersion. In this self-similar model the X-ray luminosity scales directly with velocity dispersion as  $L_X \propto \sigma_v^4$ . At cluster masses there is general agreement that observations are consistent with the self-similar picture, with numerous studies finding power law slopes consistent with  $\sim 4$  (e.g. Mulchaey & Zabludoff 1998; Helsdon & Ponman 2000a; Mahdavi & Geller 2001; Ortiz-Gil *et al.* 2004; Hilton *et al.* 2005). At group masses, however, there is some disagreement as to whether or not the  $L_X$ - $\sigma_v$  relation is merely extension of the  $\sigma_v^4$  relation found for clusters, or shallows to a slope of  $\sim 2.4$  (e.g. Helsdon & Ponman 2000b; Xue & Wu 2000).

Osmond & Ponman suggest that, rather than an actual flattening in the  $L_X$ - $\sigma_v$  relation, the observed break at group masses could be a result of  $\sigma_v$  poorly tracing the depth of the potential well. Conversely, Plionis & Tommasian (2004) argue that the observed flattening in the  $L_X$ - $\sigma_v$

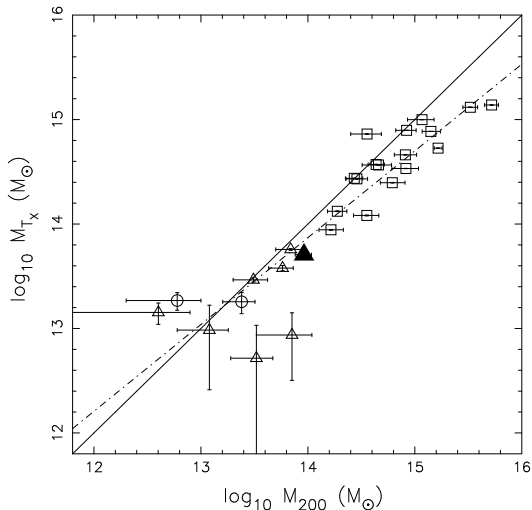


**Figure 11.** Comparison between dynamically and X-ray derived mass estimates for groups and clusters. Groups from B06 are shown with open triangles and circles, representing group and galaxy scale X-ray emission respectively. Open squares are Horner clusters with velocity dispersions measured by Girardi *et al.* (1998; see text for details). The solid line represents a one-to-one correlation, and the dashed line is a best fit to the data with a slope of  $0.83 \pm 0.08$ . Our measurements for NGC 5044 are shown as the large, filled triangle.

relation at low velocity dispersions is spurious, and is only observed as a result of a statistical bias in sampling of the low- $L_X$  limit.

Theoretically, one can predict not only the  $L_X$ - $\sigma_\nu$  correlation, but also the relationship between total mass of a system and its X-ray temperature or luminosity. Following self-similar arguments one can show that  $M \propto T_X^{3/2}$  (Afshordi & Cen 2002) and using  $L_X \propto T_X^2$ , arrive at  $L_X \propto M^{3/2}$ . As with the  $L_X$ - $\sigma_\nu$  relation, there is disagreement as to the consistency of observational data with self-similar predictions. Horner, Mushotzky & Scharf (1999) find a slope for their cluster sample consistent with the predicted power law slope of  $\sim 1.5$  in the  $M$ - $T_X$  relation, while Nevalainen *et al.* 2000 and Finoguenov, Reiprich & Böhringer (2001) find suggestions of a steeper relation, owing to the inclusion of groups in their X-ray samples. This slope change can be attributed to either an increase in the intrinsic scatter of the  $M$ - $T_X$  relation at group masses or a break in the relation where group and clusters follow fundamentally different trends.

While it is outside the scope of this paper to examine the nature of the  $L_X$ - $\sigma_\nu$  and  $L_X$ - $M$  relations in detail, it is of interest to place the NGC 5044 group in this parameter space relative to other groups and clusters. Here we adopt the GEMS and ACC samples described in §5.5.

In Figs. 12 and 13 we show the X-ray luminosity-velocity dispersion and -dynamical mass relations for the combined GEMS and ACC sample, with best fits to the GEMS, ACC and combined samples overlaid. The NGC 5044 group is fit well by both the cluster and combined sample fits in the  $L_X$ - $\sigma_\nu$  relation. While our fits suggest a difference in the group and cluster relations, the velocity dispersion measurements for low mass groups are highly uncertain (owing to their low number of member galaxies).

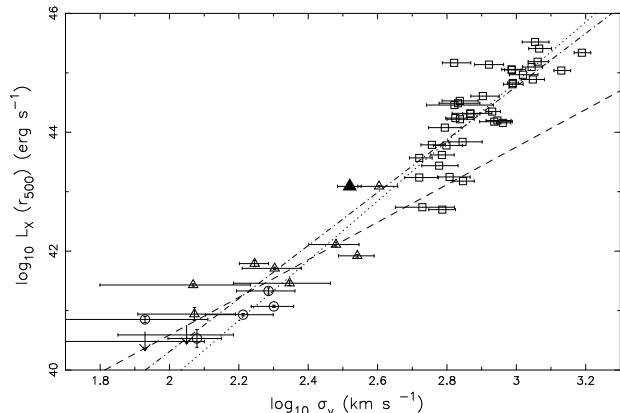


**Figure 12.** X-ray luminosity variation ( $L_X(r_{500})$ ) with velocity dispersion ( $\sigma_\nu$ ) in groups and clusters. Group and galaxy scale emission from B06 groups are shown using triangles and circles respectively. X-ray undetected groups are shown as upper limits. Open squares are Horner clusters with velocity dispersions measured by Girardi *et al.* (1998; see text for details). Our measurement of the NGC 5044 is plotted as the large, filled triangle. Dotted, dashed and dot-dashed lines represent best fits to the cluster, group and combined samples respectively.

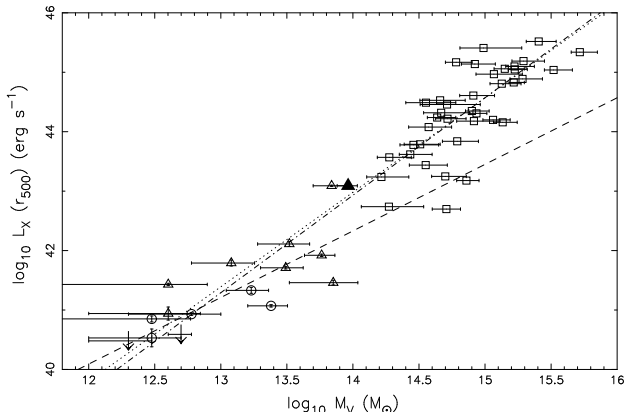


**Figure 13.** X-ray luminosity variation with dynamical mass in the groups and clusters. Symbols are the same as Fig. 12. Lines are best fits to the  $L_X$ - $M$  data and dotted, dashed and dot-dashed lines represent fits to cluster, group and combined data respectively. Dynamical masses from Girardi *et al.* (1998) have been adjusted to  $\delta=178$  (see §5.5).

The fits we find for the  $L_X$ - $M_{200}$  relation to the individual GEMS and ACC samples are consistent with the idea of a shallowing slope at group masses. As in the  $L_X$ - $\sigma_\nu$  relation, the NGC 5044 group is better fit by the ACC or combined sample trends.

Our results therefore suggest that, while the NGC 5044 group's mass of  $\sim 10^{14} M_\odot$  places it between the group and cluster regimes, the relationship of its X-ray and dynamical properties show it to be more akin to clusters than groups.

## 6 GALAXY PROPERTIES

### 6.1 Galaxy colours

With numerous studies of the photometric properties of early-type galaxies, it has been established that brighter,

more massive galaxies are increasingly redder in colour (e.g. Visvanathan & Sandage 1977; Baldry *et al.* 2004; Blanton *et al.* 2005). Further comparison of colour-magnitude relations (CMRs) between different clusters have shown nearly identical results (see, e.g. Bower, Lucy & Ellis 1992). In fact, Hogg *et al.* (2004) used a sample of SDSS galaxies to show that the slope of the CMR is roughly constant across a wide range of environments, a result that has been confirmed using larger samples from the SDSS (e.g. Gallazzi *et al.* 2006).

More detailed studies on the physical origin of the CMR have focused on comparing the stellar populations of galaxies at differing magnitudes (e.g. Bressan, Chiosi & Tantalo 1996; Gallazzi *et al.* 2006) and have found that the CMR is primarily a mass-metallicity relation. Observed trends of increased metallicity towards high masses are consistent with feedback mechanisms, such as supernova driven winds that will be increasingly efficient at blowing gas out of low mass halos and suppressing star formation from enriched gas (e.g. Trager *et al.* 2000; Thomas *et al.* 2005). The increased blueward scatter about the CMR at low masses is dominated by age effects (Gallazzi *et al.* 2006; Kodama & Arimoto 1997), where lower mass galaxies are still observed to be forming stars and higher mass galaxies are predominantly passively evolving (i.e. the “downsizing” effect).

In Fig. 14 we show the  $B - K$  vs.  $M_K$  colour-magnitude relation derived for our NGC 5044 sample. Of the four galaxies with very red colours ( $B - K > 4.6$ ), the two S0’s and spiral galaxy (open circles and spirals in Fig. 14 respectively) are seen edge on, so we expect increased reddening from dust in the disk. The fourth (elliptical) galaxy has a very large error associated with its K-band magnitude, and we suspect that the galaxy’s very red colour is due to this uncertainty.

A linear fit to the early-type galaxies gives a slope of  $-0.13 \pm 0.03$  and intercept of  $0.76 \pm 0.55$  (dashed line in Fig. 14), consistent with previous analyses of  $B - K$  CMRs (e.g. Mobasher, Ellis & Sharples 1986; Forbes *et al.* 2008). This also shows that dwarf galaxies in our sample are, on average,  $\sim 0.4$  mags bluer than the most massive galaxies.

The correlation of galaxy colours with their local density, where redder galaxies are found predominantly in higher density environments, is now a well established trend (Dressler 1980; Kauffmann *et al.* 2004; Smith *et al.* 2005; Blanton & Berlind 2007). Recent studies using large 2dFGRS and SDSS samples have found increasing evidence that local density not only correlates with galaxy colour, but also galaxy star formation properties (e.g. Lewis *et al.* 2002; Gómez *et al.* 2003). For our sample, we calculate local density for each galaxy,  $\Sigma_5$ , using the projected distance of the 5<sup>th</sup> nearest neighbour galaxy. The relationship of  $B - K$  colour with  $\Sigma_5$  is shown in Fig. 15. We note that low density outskirts of the NGC 5044 group are the most poorly sampled, and so density measurements in these regions are likely an underestimate of the true density. Nevertheless, this figure certainly suggests agreement with the findings of Lewis *et al.* (2002) and Gomez *et al.* (2003), that above a certain local density (in this case  $\Sigma_5 = 2 - 3$  galaxies  $\text{Mpc}^{-2}$ ) galaxies transition from blue and star-forming, to passively evolving and red.

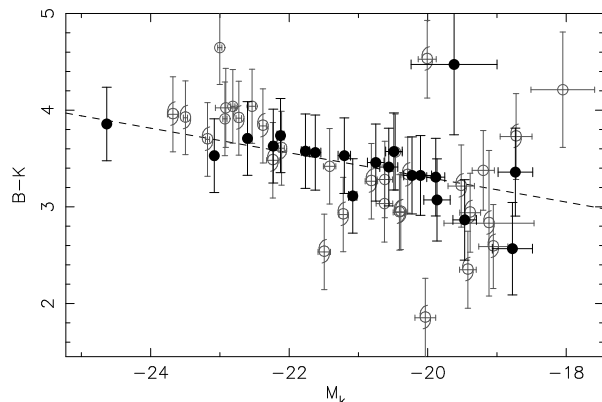


**Figure 14.**  $B - K$  vs.  $M_K$  relation for galaxies in the NGC 5044 group. Elliptical, S0 and late-type galaxies are represented by filled circles, open circles and spirals respectively. K-band errors are taken from either the 2MASS and P00 catalogues, for B-band error estimates we adopt the scatter around the best fit in Fig. 2 of 0.37 mags. The solid line is the best fit CMR to the early-type data in the sample.

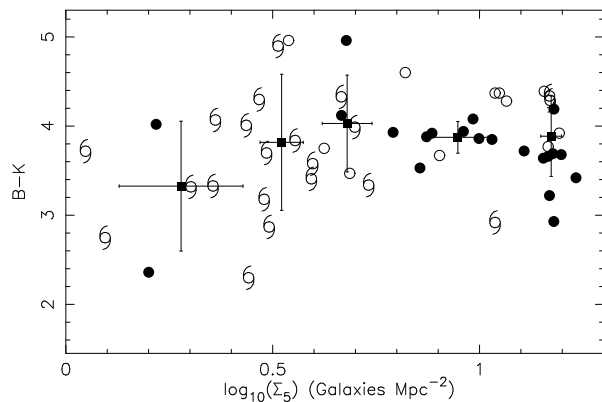


**Figure 15.**  $B - K$  vs. local density ( $\Sigma_5$ ) for galaxies in the NGC 5044 group. Symbols are the same as in Fig. 14. Squares show the mean density and colour for every 10 galaxies with  $1\sigma$  errors.

## 6.2 Spatial distribution of galaxies and segregation

With our large sample of confirmed 111 group members it is possible for us to explore the spatial and kinematic distribution of galaxies in significantly more detail than previous group studies. The most well known examples of spatial segregation, the morphology-density and morphology-radius relations (e.g. Dressler 1980; Butcher & Oemler 1984) have been well studied in galaxy clusters owing to the large numbers of galaxies typically available relative to the group environment. However studies focusing on galaxy groups also find significant evidence for segregation. In addition to spatial segregation, galaxies in clusters are found to be dynamically segregated with respect to both luminosity and morphology in simulations (Yepes *et al.* 1991; Fusco-Femiano & Menci 1998), which is supported by observations of dynamical segregation in both groups and clusters (Girardi *et al.* 2003; Lares *et al.* 2004).

Here we examine evidence for both spatial and dynamical segregation amongst our galaxy group sample.

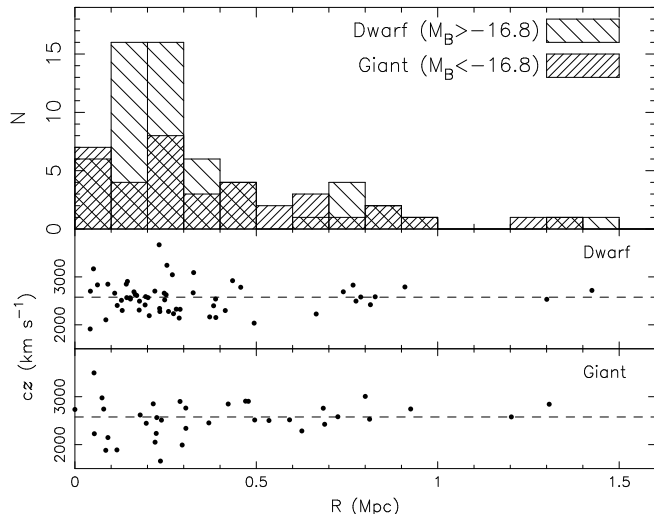


**Figure 16.** Histogram showing number of galaxy type, either dwarf or giant, with projected radius. Second and third panels show recession velocity vs. projected radius for dwarf and giant sub-samples respectively. Dashed lines in panels two and three show the mean group velocity of  $2577 \text{ km s}^{-1}$ .

### 6.2.1 Spatial segregation

To address the question of spatial segregation we subdivide our total sample by morphology (early- vs. late-types) and luminosity (where  $M_B = -16.8$  mag is used as the break between dwarf and giant galaxies), the results of which are shown in Figs. 16 and 17.

When split by luminosity (Fig. 16), galaxies show no significant evidence for a radial bias, i.e. the two luminosity sub-samples are similarly distributed with radius. The hypothesis that dwarf and giant galaxies have the same radial distribution is only marginally rejected at the 70 percent level by a Kolmogorov-Smirnov (KS) test, confirming the visually apparent lack of a strong radial bias with luminosity. This is consistent with the known trend in dwarf-to-giant ratios (DGR) for groups and clusters, where the DGR is independent of position observed in the group (see e.g. FS91).

Splitting galaxies based on morphology (Fig. 17) gives a markedly different result in that galaxies are differently distributed at the  $5 \sigma$  level as determined using a KS test. This is consistent with expectations from the morphology-density and morphology-radius relations (Butcher & Oemler 1976; Dressler 1980) and our findings from §6.1.

It is important to keep in mind that our group sample is assembled from a variety of sources with differing spatial coverage, selection and completeness (see Fig. 5 and §3), all of which could be inducing a radial bias in the results presented in Figs. 16 and 17. In particular, the region within  $\sim 600$  kpc of the group center (approximately the area covered by FS90 and, therefore, our AAOmega observations) includes significant numbers of faint (dwarf) galaxies that are likely not included in the samples at larger radii. Repeating the KS test on only galaxies within the central 600 kpc gives similar results to those above; dwarf and giant galaxies appear similarly distributed (at the  $\sim 60$  percent level) while early- and late-type galaxies show a difference in their radial distributions significant at the  $3 \sigma$  level.

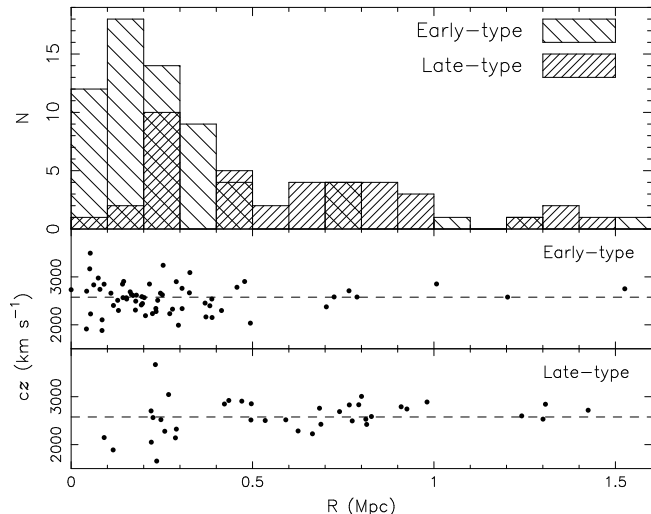


**Figure 17.** Same as Fig. 16, except galaxies are divided by morphology (early- vs. late-type) rather than luminosity.

### 6.2.2 Dynamical segregation

The dynamical segregation of galaxies in the NGC 5044 group has been examined previously by Cellone & Buzzoni (2005) using a sample of 26 early- and late-type galaxies. When dividing their sample based on morphology, they find early- and late-type galaxies exhibit velocity dispersions that differ at the 93 percent level (as measured using an  $F$  test). Cellone & Buzzoni (2005) find no evidence for luminosity segregation in their early-type galaxies, however were unable to examine luminosity segregation between their early- and late-type samples due to low numbers of late-type galaxies.

Here we revisit the question of dynamical segregation in the NGC 5044 group using the morphology and luminosity sub-samples described above. We then compare the line-of-sight velocity distributions of sub-samples using two different methods to look for dynamically distinct behaviour. The first comparison is carried out using a KS test, which computes the likelihood of the two different samples being drawn from the same parent velocity distribution. The second test we use is an  $F$ -test, which gives the likelihood of the two distributions having significantly different variances. Table 5 summarises the results of the KS and  $F$ -test for our luminosity and morphology sub-samples.

Our results for morphological segregation computed using the  $F$ -test are consistent with Cellone & Buzzoni (2005), however increasing the sample of galaxies from 26 to 105 has decreased the significance slightly. There is marginal evidence of a variation in the distributions of early-type dwarf vs. giant galaxies and amongst early- vs. late-type dwarf galaxies, however these results are of low statistical significance ( $\sim 1.6\sigma$ ).

When split by either luminosity or morphology our sample of NGC 5044 group galaxies is remarkably homogeneous, showing little strong evidence for any dynamical segregation. Results from the KS test show no evidence that any of the sub-samples are statistically different distributions. In fact, the results for early- vs. late-type galaxies seem to suggest that the two distributions are actually *similar* at the  $\sim 2\sigma$  level. Giant ( $M_B < -17$ ) galaxies in our sample are similar

**Table 5.** Results from tests for dynamical segregation.

| Sample  | Sub-sample             | N <sub>1</sub> | N <sub>2</sub> | $c\bar{z}_1$<br>(km s <sup>-1</sup> ) | $\sigma_1$<br>(km s <sup>-1</sup> ) | $c\bar{z}_2$<br>(km s <sup>-1</sup> ) | $\sigma_2$<br>(km s <sup>-1</sup> ) | L <sub>KS</sub> | L <sub>F</sub> |
|---|------------------------|----------------|----------------|---------------------------------------|-------------------------------------|---------------------------------------|-------------------------------------|-----------------|----------------|
| (1)   | (2)                    | (3)            | (4)            | (5)                                   | (6)                                 | (7)                                   | (8)                                 | (9)             | (10)           |
| <i>Luminosity Segregation</i>                     |                        |                |                |                                       |                                     |                                       |                                     |                 |                |
| M <sub>B</sub> < -16.8 vs. M <sub>B</sub> > -16.8 | all morphologies       | 37             | 58             | 2542±71                               | 397±71                              | 2540±40                               | 302±36                              | 46.1            | 84.8           |
| M <sub>B</sub> < -16.8 vs. M <sub>B</sub> > -16.8 | late-type              | 18             | 17             | 2492±108                              | 438±104                             | 2580±77                               | 317±64                              | 27.6            | 8.7            |
| M <sub>B</sub> < -16.8 vs. M <sub>B</sub> > -16.8 | early-type             | 19             | 41             | 2582±79                               | 380±67                              | 2522±53                               | 296±38                              | 67.8            | 91.9           |
| <i>Morphological Segregation</i>                  |                        |                |                |                                       |                                     |                                       |                                     |                 |                |
| early- vs. late-types                             | all luminosities       | 60             | 35             | 2542±48                               | 317±38                              | 2547±61                               | 380±59                              | 16.7            | 90.8           |
| early- vs. late-types                             | M <sub>B</sub> > -16.8 | 41             | 17             | 2522±53                               | 296±38                              | 2580±77                               | 317±64                              | 76.4            | 94.0           |
| early- vs. late-types                             | M <sub>B</sub> < -16.8 | 19             | 18             | 2582±79                               | 368±67                              | 2492±108                              | 438±104                             | 41.6            | 8.5            |

Notes. Columns are as follows: (1) and (2) describe the samples being compared. (3) and (4) give the number of galaxies in each sub-sample. (6)–(8) give the mean velocities and dispersions of the two different sub-samples. (9) is the significance, from a K-S Test, that the two distributions are drawn from different distributions. (10) gives the significance, via an F-test, that the distributions have different variances.

with respect to their dynamics in the group irrespective of morphological type.

## 7 DISCUSSION AND CONCLUSIONS

We have used multi-object spectroscopy to obtain recession velocity measurements for galaxies in the NGC 5044 group. Combining these new observations with available data from literature we are able to define the NGC 5044 group as containing 111 members with  $M_B \leq -13.5$  mags, nearly a three-fold increase over previous numbers of confirmed group members.

An analysis of common dynamical indicators such as crossing time, line-of-sight velocity distribution, position of the X-ray peak relative to the centroid suggest that the NGC 5044 group is relaxed and virialized despite the observed 150 km s<sup>-1</sup> peculiar velocity of the brightest group galaxy NGC 5044. This conclusion of virialization is consistent with XMM X-ray contours for the group, which are very regular and undisturbed. We note, however, that none of our tests for virialization are sensitive to effects along the line-of-sight, and so the true dynamical state of the group remains somewhat unknown. Taking the above indicators at face value, however, the group’s virialization suggests that the NGC 5044 group has experienced no *major* sub-group mergers in several crossing times ( $\sim 1$  Gyr).

While the dynamical indicators discussed above will give hints as to the timescale of major merger activity, it is likely that low-mass sub-group mergers will not significantly disrupt the virialization of the system as determined via these indicators. By computing the Dressler-Shectman  $\Delta$  statistic, we have been able to visually and statistically search for space-velocity substructure in the group. In doing so, we find evidence for a low mass substructure  $\sim 1.4$  Mpc from NGC 5044 group centre.

Two body interactions are expected to lead to dynamical and luminosity segregation in mature groups such as NGC 5044 (e.g. Fusco-Femiano & Menci 1998; Lares *et al.* 2004). In examining the NGC 5044 group’s galaxy population however, we find that galaxies are primarily segregated with respect to their morphologies, and there is no

*strong* evidence for segregation in either dynamics or luminosity.

While luminosity segregation is an expected outcome of mergers in groups (e.g. Fusco-Femiano & Menci 1998; Lares *et al.* 2004), Ludlow *et al.* (2007) have used N-body simulations to show that it is possible to eject sub-halos from a group, via multi-body interactions, resulting in significant numbers of associated sub-halos<sup>2</sup> residing in the outskirts of the group (as far as 5 times the virial radius). In relaxed groups such as NGC 5044, galaxies have had significant time for two-body interactions to take place, and so the ejection of galaxies from the group centre is more likely to wash out segregation trends. In addition, this complicates the common interpretation of group-centric radius as a tracer of accretion history as it is no longer clear that galaxies in the outskirts are actually the most recent galaxies to have been accreted into the group potential.

Early-type galaxies in the NGC 5044 group are well described by a linear  $B-K$  colour-magnitude relation, and are consistent with previous interpretations for the slope in the CMR due to decreasing metallicity or age at lower galaxy masses. Correlations of  $B-K$  colour with local density seem to further suggest that the majority of these bluer, fainter galaxies are residing in the outskirts of the group, where densities are less than 2 – 3 galaxies Mpc<sup>-2</sup>. This is consistent with findings for groups and cluster outskirts in the 2dFGRS and SDSS surveys (e.g. Lewis *et al.* 2002; Gomez *et al.* 2003), however our low sample size prohibits a more quantitative analysis of this effect.

Future work will include a consideration of stellar populations in the galaxies of the NGC 5044 group, measured using a combination of our AAOmega and 6dFGS spectra. Combining the dynamical and kinematic data of the confirmed group members presented here with age and metallicity measurements will allow us to approach the analysis of this group and its galaxy population in significantly more detail than previously attainable. In particular, the expectation of pre-processing in groups implies a necessary chemo-dynamical distinction between galaxies associated with the

<sup>2</sup> Ludlow *et al.* (2007) define associated halos as those that have, at some point, passed within the virial radius of the central halo

group and field galaxies entering the group environment for the first time.

## ACKNOWLEDGEMENTS

The authors would like to thank Sergio Cellone for his helpful comments and suggestions. We acknowledge the analysis facilities provided by IRAF, which is distributed by the National Optical Astronomy Observatories, which is operated by the Association of Universities for Research in Astronomy, Inc., under cooperative agreement with the National Science Foundation.

This publication makes use of data products from the Two Micron All Sky Survey, which is a joint project of the University of Massachusetts and the Infrared Processing and Analysis Center/California Institute of Technology, funded by the National Aeronautics and Space Administration and the National Science Foundation. We also thank the Australian Research Council for funding that supported this work.

## REFERENCES

- Adami C., Biviano A., Mazure A., 1998, *A&A*, 331, 439  
 Afshordi N., Cen R., 2002, *ApJ*, 564, 669  
 Baldry I. K., Glazebrook K., Brinkmann J., Ivezić Ž., Lupton R. H., Nichol R. C., Szalay A. S., 2004, *ApJ*, 600, 681  
 Beers T. C., Flynn K., Gebhardt K., 1990, *AJ*, 100, 32  
 Betoya-Nonesca J. G., Fukazawa Y., Ohsugi T., 2006, *PASJ*, 58, 103  
 Biviano A., Girardi M., 2003, *ApJ*, 585, 205  
 Biviano A., Katgert P., 2004, *A&A*, 424, 779  
 Biviano A., Katgert P., Thomas T., Adami C., 2002, *A&A*, 387, 8  
 Blanton M. R., Berlind A. A., 2007, *ApJ*, 664, 791  
 Blanton M. R., Eisenstein D., Hogg D. W., Schlegel D. J., Brinkmann J., 2005, *ApJ*, 629, 143  
 Bower R. G., Lucey J. R., Ellis R. S., 1992, *MNRAS*, 254, 589  
 Bressan A., Chiosi C., Tantalo R., 1996, *A&A*, 331, 425  
 Brough S., Forbes D. A., Kilborn V. A., Couch W., 2006a, *MNRAS*, 370, 1223 (B06)  
 Brough S., Forbes D. A., Kilborn V. A., Couch W., Colless M., 2006b, *MNRAS*, 369, 1351  
 Bryan G. L., Norman M. L., 1998, *ApJ*, 495, 80  
 Buote D. A., Lewis A. D., Brighenti F., Mathews W., 2003, *ApJ*, 594, 741  
 Buote D. A., Brighenti F., Mathews W. G., 2004, *ApJ*, 607, 91  
 Bureau M., Carignan C., 2002, *AJ*, 123, 1316  
 Burgett W. S. *et al.*, 2004, *MNRAS*, 352, 605  
 Butcher H., Oemler A Jr., 1984, *ApJ*, 285, 426  
 Carlberg R. G. *et al.*, 1997, *ApJ*, 485, 13  
 Carlberg R. G., Yee H. K. C., Ellingson E., 1997, *ApJ*, 478, 462  
 Carlberg R. G., Yee H. K. C., Morris S. L., Lin H., Hall P. B., Patton D. R., Sawicki M., Shepherd C. W., 2001, *ApJ*, 552, 427  
 Cellone S. A., Buzzoni A., 2005, *MNRAS*, 356, 41  
 David L. P., Jones C., Froman W., Daines S., 1994, *ApJ*, 428, 544  
 den Hartog R., Katgert P., 1996, *MNRAS*, 279, 349  
 Diaferio A., Ramella M., Geller M. J., Ferrari A., 1993, *AJ*, 105, 2035  
 Dressler A. J., 1980, *ApJ*, 236, 351  
 Dressler A., Shectman S. A., 1988, *AJ*, 95, 985  
 Dubinski J., Carlberg R. G., 1991, *ApJ*, 378, 496  
 Eke V. R. *et al.*, 2004, *MNRAS*, 348, 866  
 Ferguson H. C., Sandage A., 1990, *AJ*, 100, 1 (FS90)  
 Ferguson H. C., Sandage A., 1991, *AJ*, 101, 765 (FS91)  
 Finoguenov A., Reiprich T. H., Böhringer H., 2001, *A&A*, 368, 749  
 Forbes D., Laskey P., Graham A., Spitler L., 2008, preprint (astro-ph/0806.1090v2)  
 Fujita Y., 2003, *PASJ*, 55, 593  
 Fukazawa Y., 1997, Ph.D. thesis, Univ. Tokyo  
 Fusco-Femiano R., Menci N., 1998, *ApJ*, 498, 95  
 Gallazzi A., Charlot S., Brinchmann J., White S. D. M., 2006, *MNRAS*, 370, 1106  
 Geller M. J., Huchra J. P., 1983, *ApJS*, 52, 61  
 Girardi M., Escalera E., Fadda D., Giuricin G., Mardirossian F., Mezzetti M., 1987, *ApJ*, 482, 41  
 Girardi M., Fadda D., Giuricin G., Mardirossian F., Mezzetti M., Biviano A., 1996, *ApJ*, 457, 61  
 Girardi M., Giuricin G., Mardirossian F., Mezzetti M., Boschin W., 1998, *ApJ*, 505, 74  
 Girardi M., Rigoni E., Mardirossian F., Mezzetti M., 2003, *A&A*, 406, 403  
 Gómez P. L. *et al.*, 2003, *ApJ*, 584, 210  
 Gunn J. E., Gott J. R., 1972, *ApJ*, 176, 1  
 Helsdon S. F., Ponman T. J., 2000a, *MNRAS*, 315, 356  
 ———, 2000b, *MNRAS*, 319, 933  
 Hernquist L., 1990, *ApJ*, 356, 359  
 Hester J. A., 2006, *ApJ*, 647, 910  
 Hilton M. *et al.*, 2005, *MNRAS*, 363, 661  
 Hogg D. W. *et al.*, 2004, *ApJ*, 601, 29  
 Horner D. J., Mushotzky R. F., Scharf C. A., 1999, *ApJ*, 520, 78  
 Horner D. J., 2001, Ph.D. thesis, Univ. of Maryland, College Park  
 Huchra J. P., Geller M. J., 1982, *ApJ*, 257, 423  
 Hwang H. S., Lee M. G., 2008, *ApJ*, 676, 218  
 Jarrett T. H., Chester T., Cutri R., Schneider S., Skrutskie M., Huchra J. P., 2000, *AJ*, 119, 2498  
 Jensen J. B., Tonry J. L., Barris B. J., Thompson R. I., Liu M. C., Rieke M. J., Ajhar E. A., Blakeslee J. P., 2003, *ApJ*, 583, 712  
 Jones D. H., Saunders W., Read M., Colless M., 2005, *PASA*, 22, 277  
 Kantharia N. G., Ananthkrishnan S., Nityananda R., Hota A., 2005, *A&A*, 435, 483  
 Kauffmann G., White S. D. M., Heckman T. M., Ménard B., Brinchmann J., Charlot S., Tremonti C., Brinkmann J., 2004, *MNRAS*, 353, 713  
 Kodama T., Arimoto N., 1997, *A&A*, 320, 41  
 Kodama T., Smail I., 2001, *MNRAS*, 326, 637  
 Lares M., Lambas D. G., Sánchez A. G., 2004, *MNRAS*, 352, 501  
 Lewis I. *et al.*, 2002, *MNRAS*, 334, 673  
 Ludlow A. D., Navarro J. F., Springel V., Jenkins A., Frenk C. S., Helmi A., 2008 preprint (astro-ph/0801.1127v1)  
 Lynden-Bell D., 1967, *MNRAS*, 136, 101  
 Mahdavi A., Geller M. J., 2001, *ApJ*, 554, 129  
 McKay N. P. F. *et al.* 2004, *MNRAS*, 352, 1121  
 Merritt D., 1988, in Dickey J., ed., *ASP Conf. Ser. Vol. 5., The Minnesota Lectures on Clusters of Galaxies and Large-Scale Structures*, Astron. Soc. Pac., San Francisco, p. 175  
 Miles T. A., Raychaudhury S., Forbes D. A., Goudfrooij P., Ponman T. J., Kozhurina-Platais V., 2004, *MNRAS*, 355, 785  
 Mobasher B., Ellis R. S., Sharples R. M., 1986, *MNRAS*, 223, 11  
 Moore B., Katz N., Lake G., Dressler A., Oemler A., 1996, *Nature*, 379, 613  
 Mulchaey J. S., Zabludoff A. I., 1998, *ApJ*, 496, 73  
 Navarro, J. F., Frenk C. S., White S. D. M., 1995, *MNRAS*, 275, 56  
 ———, 1996, *ApJ*, 462, 563  
 ———, 1997, *ApJ*, 490, 493  
 Nevalainen J., Markevitch M., Forman W., 2000, *ApJ*, 532, 694

- Niemi S., Nurmi P., Heinämäki P., Valtonen M., 2007, MNRAS, 382, 1864
- Nolthenius R., White S. D. M., 1987, MNRAS, 225, 505
- Oegerle W. R., Hill J. M., 2001, AJ, 122, 2858
- Ortiz-Gil A., Guzzo L., Schuecker P., Böringer H., Collins C. A., 2004, MNRAS, 348, 3250
- Osmond J. P. F., Ponman T. J., 2004, MNRAS, 350, 1511
- Paturel G., Fang Y., Petit C., Garnier R., Rousseau J., 2000, A&AS, 146, 19 (P00)
- Paturel G., Vauglin I., Petit C., Borsenberger J., Epchtein N., Fouqué P., Mamon G., 2005, A&A, 430, 751 (P05)
- Pinkney J., Roettiger K., Burns J. O., Bird C. M., 1996, ApJS, 104, 1
- Plionis M., Tovmassian H. M., 2004, A&A, 416, 441
- Poole G. B., Fardal M. A., Babul A., McCarthy I. G., Quinn T., Wadsley J., 2006, MNRAS, 373, 881
- Ramella M., Geller M. J., Huchra J. P., 1989, ApJ, 344, 57
- Ramella M. *et al.*, 2007, A&A, 470, 39
- Rasmussen J., Ponman T. J., Mulchaey J. S., 2006, MNRAS, 370, 453
- Schlegel D. J., Finkbeiner D. P., Davis M., 1998, ApJ, 500, 525
- Skrutskie M. F., *et al.*, 2006, AJ, 131, 1163
- Smith G. P., Treu T., Ellis R. S., Moran S. M., Dressler A., 2005, ApJ, 620, 78
- Tamura T., Kaastra J. S., Makishima K., Takahashi I., 2003, A&A, 339, 497
- Thomas D., Maraston C., Bender R., Mendes de Oliveira C., 2005, ApJ, 621, 673
- Tonry J. L., Dressler A., Blakeslee J. P., Ajhar E. A., Fletcher A. B., Luppino G. A., Metzger M. R., Moore C. B., 2001, ApJ, 546, 681
- Trager S. C., Faber S. M., Worthey G., González J. J., 2000, AJ, 120, 165
- Trentham N., Tully R. B., 2002, MNRAS, 335, 712
- Visvanathan N., Sandage A., 1977, ApJ 216, 214
- Weinmann S. M., van den Bosch F. C., Yang X., Mo H. J., 2006, MNRAS, 366, 2
- West M. J., Oemler A. Jr., Dekel A., 1998, ApJ, 327, 1
- Xue Y., Wu X., 2000, ApJ, 538, 65
- Yepes G., Dominguez-Tenreiro R., del Pozo-Sanz R., 1991, ApJ, 373, 336
- Zabludoff A. I., Franx M., Geller M. J., 1993, ApJ, 419, 47
- Zabludoff A. I., Mulchaey J. S., 1998, ApJ, 496, 39

## APPENDIX A: DYNAMICAL FORMULAE

Virial mass,  $M_V$ , has been calculated using the virial mass estimator from Heisler *et al.* (1985)

$$M_V = \frac{3\pi N}{2G} \frac{\sum_i \nu_{i,gc}^2}{\sum_{i<j} 1/R_{gc,ij}}, \quad (\text{A1})$$

where  $\nu_{i,gc}$  is the velocity of galaxy  $i$  with respect to the group centroid and  $R_{gc,ij}$  is the projected group-centric separation from other galaxies.

Velocity dispersion is calculated using the biweight scale estimator (Beers *et al.* 1990)

$$\sigma_\nu = n^{1/2} \frac{\left[ \sum_{|u_i|<1} (\nu_i - \bar{\nu})^2 (1 - u_i^2)^4 \right]^{1/2}}{\left| \sum_{|u_i|<1} (1 - u_i^2)(1 - 5u_i^2) \right|}, \quad (\text{A2})$$

where  $\nu_i$  denotes the recession velocity of the  $i^{th}$  galaxy and  $\bar{\nu}$  is the median group velocity  $u_i$  is defined as

$$u_i = \frac{(\nu_i - \bar{\nu})}{c \text{MAD}}, \quad (\text{A3})$$

with MAD being the median absolute deviation (median deviation of the sample with respect to the sample median). Where we calculate the velocity dispersion for low numbers of galaxies ( $< 15$ ), we use the gapper algorithm of Beers *et al.* (1990),

$$\sigma_\nu = \frac{\sqrt{\pi}}{n(n-1)} \sum_{i=1}^{n-1} w_i g_i, \quad (\text{A4})$$

where  $w_i = i(n-i)$  and  $g_i = z_{i+1} - z_i$ . This has been shown to be more efficient for low sample sizes than the biweight estimator (Beers *et al.* 1990).

The  $r_{500}$  radius has been calculated using the velocity dispersion via

$$r_{500} = \frac{0.096\sigma_\nu}{H_0}. \quad (\text{A5})$$

The crossing time is defined as

$$t_c = \frac{3r_H}{5^{3/2}\sigma_\nu}, \quad (\text{A6})$$

in units of  $H_0^{-1}$ .  $r_H$  is the mean harmonic radius (Ramella *et al.* 1989) given by

$$r_H = \pi D \sin \left[ \frac{1}{2} \frac{n(n-1)}{2 \sum_i \sum_{j>i} \theta_{ij}^{-1}} \right], \quad (\text{A7})$$

where  $D$  represents the distance to the group and  $\theta_{ij}$  is the projected angular separation between galaxies  $i$  and  $j$ .